Università degli Studi di Perugia

DEPARTMENT OF PHYSICS AND GEOLOGY
Master Degree in Physics

MASTER DEGREE THESIS

Towards reconstruction of large-scale matter power spectrum: a study of the impact on cosmological constraints on massive neutrinos from future large-scale-structure surveys

Candidate
Francesco Sorrenti

Supervisor
Prof. Emanuele Fiandrini

External supervisor
Dr. Martina Gerbino

Academic year 2020-2021

All'Amor che move il Sole
e l'altre Stelle

Per nonno

Contents

Introduction

Since the first pioneering work by P.J.E. Peebles in the seventies [39], the study of cosmological perturbations has improved more and more in the last decades. In terms of matter perturbations we can define the matter power spectrum $P_m(k, z)$, with k the momentum magnitude and z the redshift. It is one of the key elements in understanding our Universe, its components and evolution. Surveys as *SDSS* [11] have given important contributions in enriching our knowledge about $P_m(k, z)$. In the next years many surveys will be launched. One of the most important is *Euclid* [1], whose launch is planned for 2022.

Measuring the distribution of matter on large scale is one of the goals of Euclid and future cosmological surveys. It could provide information about many issues such as the total matter density, the primordial power spectrum, the nature and properties of dark energy and anomalies in the cosmic microwave background (CMB) [33].

Actually, performing these measurements at very large scales is difficult due to many experimental limits. Therefore, in the last years procedures for reconstructing indirectly the large scale structure have been proposed. Among these, the Refs. [33] [32], published last year, propose to do it using information about how the large scale structures affect the small scales. It is a new and absolutely interesting framework that seems to be really fruitful, as the present work is going to show.

We will realize a simplified yet stand-alone pipeline to study the impact of introducing information from large scales on cosmological constraints in an extended cosmological model with massive neutrinos. Massive neutrinos affect the evolution of matter perturbations in a peculiar way. We want to test the improvement that can come from the inclusion of large scales when constraining the sum of neutrino masses $\sum m_\nu$ with P_m.

To this scope, we first produce a synthetic dataset based on Euclid specifications. Then, we write a code to perform a Monte Carlo Markov Chain (MCMC) analysis to constrain cosmological parameters. Finally, we compare the results obtained with and without large scales.

This thesis is organized as follows:

1. we start rewieving the Standard Cosmological model and its extension

in term of the sum of neutrinos masses $\sum m_\nu$ in Chapter 1;

2. we focus on the neutrino cosmic history and its impact on the cosmic evolution in Chapter 2;

3. we define the matter power spectrum underlining its dependence on the cosmological parameter, in particular on $\sum m_\nu$ in Chapter 3;

4. we introduce the formalism of large scale structure reconstruction and light cone matter power spectrum in Chapter 4;

5. in Chapter 5 we apply the formalism introduced in the previous chapters to the *Euclid* survey as a case study. We refer to Ref. [10] for Euclid specifications.

Before moving to discuss our work, let us underline its original products:

- a Mathematica code for the reconstruction of the matter power spectrum at large scale using information from a fiducial matter power spectrum at small scale computed via the Einstein-Boltzmann solver *CAMB* [2];

- a Python code with the definition of the likelihood function used in the MCMC analysis. It has been developed in order to be compatible with the *Cobaya* software [15] used for bayesian analysis and run on a HPC cluster provided by CINECA.

- a Python code (in Jupyter Notebook) for the statistical analysis of the MCMC results using the software *GetDist* [3];

- a Python code (in Jupyter Notebook) for the study of the impact of the cosmological parameters on the matter power spectrum.

Chapter 1

The Standard Model of Cosmology

1.1 What is a cosmological model

A cosmological model describes the evolution and the characteristics of the Universe, taking into account three important elements:

1. cosmological principle: the Universe at large scale is homogeneous and isotropic;
2. gravitation: it is the dominant interaction at large scale described by the General Relativity;
3. expansion of the Universe: according to the Hubble-Lemaître Law our Universe is expanding in each own part. On a first approximation, an observer see a body distant d recessing from them with a velocity:

$$v = H_0 d, \tag{1.1}$$

where H_0 is the Hubble-Lemaître constant. Coming back in time, this implies that our universe expanded from an extreme dense singularity, from which the term "*Big Bang*". This is even confirmed by many observations probing the theoretical predictions, in particular Supernovae, the abundance of light elements from Big-Bang Nucleosynthesis and the Cosmic Microwave Background.

1.2 The Standard Model of Cosmology

The cosmological model commonly accepted today, the Standard Model of Cosmology (SMC), is based theoretically upon the General Theory of Relativity (GTR), which describes the physics of very large scales in a classical

scenario, and the Standard Model of Particle Physics (SMPP), which describes the infinitely small in a quantum scenario [41].

Let us focus on the Einstein's Gravitational Field Equations. They relate the space-time geometry with the presence of energy-momentum source:

$$R_{\mu\nu} - \frac{1}{2}Rg_{\mu\nu} = -8\pi G\left(T_{\mu\nu} - \frac{\Lambda}{8\pi G}g_{\mu\nu}\right), \tag{1.2}$$

where $R_{\mu\nu}$ is the Ricci tensor describing the space-time geometry, G is Newton's gravitation constant, Λ is a constant called *Cosmological Constant*, $g_{\mu\nu}$ is the metric tensor and $T_{\mu\nu}$ is the energy-momentum tensor.

A solution for (1.2) is given by the Friedmann-Lemaître-Robertson-Walker (FLRW) metric:

$$ds^2 = dt^2 - a^2\left[\frac{dr^2}{1-kr^2} + r^2(d\theta^2 + \sin^2\theta d\varphi^2)\right]^1, \tag{1.3}$$

where k is the curvature parameter describing the spatial curvature of the universe. According to the cosmological principle, the universe is described as a quiet perfect fluid in a time-evolving comoving system with a scale factor $a = a(t)$ which, in agreement with the expansion of the Universe, increases over t. In this thesis we will follow the common practice of normalizing the scale factor at the present time t_0, so that $a(t_0) = a_0 = 1$. Concerning the k parameter, there are three possibilities [13]:

- $k < 0$: negative curvature, also called closed;
- $k = 0$: no curvature, also called flat;
- $k > 0$: negative curvature, also called open.

Using this metric in (1.2) we get the Friedmann equations:

$$H^2 = \left(\frac{\dot{a}}{a}\right)^2 = \frac{8\pi G}{3}\rho - \frac{k}{a^2}, \tag{1.4a}$$

$$\frac{\ddot{a}}{a} = -\frac{4\pi G}{3}(\rho + 3p). \tag{1.4b}$$

According to k and to the nature of the energy density ρ of the cosmic fluid, we get different solutions describing different cosmological models.

[1] In all our dissertation we will use natural units (i.e. $c = k_B = \hbar = 1$) and the metric signature $(+---)$

For a complete description, we should take into account the following equation:

$$\dot{\rho} + 3(\rho + p)\frac{\dot{a}}{a} = 0 \tag{1.5}$$

deriving from the continuity equation $T^{\mu\nu}_{;\mu} = 0$ and the equation of state:

$$p = w\rho \tag{1.6}$$

where w depends on the characteristics of the energy density: it is equal to -1, 0, 1/3 for cosmological constant, radiation and matter respectively.

If w is constant, using (1.6) we get from (1.5) that:

$$\rho \propto a^{-3(1+w)}. \tag{1.7}$$

As a consequence:

- $\rho =$ *constant* for cosmological constant;
- $\rho \propto a^{-3}$ for matter;
- $\rho \propto a^{-4}$ for radiation.

Just from these approximated results, remembering that a is increasing over time, we can distinguish in the Universe evolution:

1. the Radiation-Dominated (RD) era in the early Universe;
2. the Matter-Dominated (MD) era;
3. the Dark-Energy-dominated (DE) era until the present time.

We can always define the critical density

$$\rho_{crit}(t) = \frac{3H^2}{8\pi G} \tag{1.8}$$

that, as we will see in Sec.1.4, it is useful to reformulate the Friedmann Equation (1.4a).

1.3 Cosmological perturbations

It is important to underline that the results we have got until now concern just the evolution of the cosmological background, i.e. the average values. We focused on a “smooth” universe with homogenous density. Actually, the universe is not so.
In fact, both the CMB anisotropies and the matter perturbations, which are

the main cosmological observables, can be analysed introducing cosmological perturbations, which describe the deviations from the average density and the corresponding deviations from the Hubble expansion velocity.

The cosmological perturbations are supposed to be caused by primordial quantum fluctuations which expanded to macroscopic proportion during the inflationary epoch [56].
The inflationary epoch is a period between 10^{-36}s and 10^{-34}s after the Big Bang during which the universe inflates, i.e. it goes under an accelerated expansion and expands exponentially its dimensions [25].

The evolution of the cosmological perturbations can be studied with the Einstein-Boltzmann equations [18], a set of six differential equations obtained perturbing the Einstein's Equations (1.2) and the Boltzmann equations describing the behaviour of matter and radiation.

1.4 The ΛCDM model

According to currently available observations, the best description of the Universe is provided by the ΛCDM model, where [44]:

- Λ stands for the fact that the dominant energy density of the Universe at the present time (the Dark Energy) behaves like vacuum energy, i.e. like the cosmological constant of the general relativity;
- CMD stands for the fact that the matter is mainly composed by collisionless not relativistic components known as Cold Dark Matter (CDM) which don't react electromagnetically.

If we consider cold dark matter (c), baryons (alias ordinary matter) (b), photons (γ), dark energy (Λ), massive neutrinos (ν) and a curvature component Ω_k, using (1.7) and (1.8) we can rewrite (1.4a) as:

$$H^2(a) = H_0^2\left[(\Omega_c + \Omega_b)\, a^{-3} + \Omega_\gamma\, a^{-4} + \Omega_\Lambda + \Omega_k\, a^{-2} + \frac{\rho_\nu}{\rho_{crit,0}}\right], \qquad (1.9)$$

where Ω_n is the n-eth present-day dimensionless density parameter defined as $\Omega_n = \rho_{n,0}/\rho_{crit,0}$ and the subscript "0" means that we refer to quantities evaluated at the present time (we omit this subscript for Ω_n from the moment we will consider just present-day density parameters)

Actually, Ω_k is not a energy density. It is a fictitious "curvature" density defined as:

$$\Omega_k = -\frac{k}{{H_0}^2}. \qquad (1.10)$$

It is important to underline that, because neutrino equation of state has not a constant parameter w, it is not possible in general to isolate the "a"- dependence and to write the analogous $\Omega_{\nu,tot}$, where the subscript "tot" refers to the fact that we consider the sum over all possible neutrino mass eigenstates.

The sum of the density parameters is normalized:

$$\sum_n \Omega_n = 1, \tag{1.11}$$

as we can see from (1.9) putting $a = a_0 = 1$ [26].

A dimensionless Hubble constant h is commonly used. In this way, the Hubble constant can be expressed as:

$$H_0 = h\ 100 \frac{\text{km}}{\text{s Mpc}}. \tag{1.12}$$

and consequently we get a dimensionless formulation of (1.9):

$$h^2(z) = (\omega_c + \omega_b)(1+z)^3 + \omega_\gamma(1+z)^4 + \omega_\Lambda + \omega_k(1+z)^2 + \frac{8\pi G}{3}\rho_\nu(z), \tag{1.13}$$

where we introduced the redshift z using the definition $(1 + z) = a^{-1}$ and the quantity $\omega_i = \Omega_i h^2$ referred to the i-eth density component.

The ΛCMD model is called "Concordance Cosmological Model" because independent and different cosmological observations result in concordant constraints, as it is reported in the figure 1.1

It is interesting to underline that, in its simplest version, the ΛCDM model needs just six parameters [44] to describe statistically our universe that, in this first approximation and in agreement with data [59], is considered spatially flat ($\Omega_k = 0$). In this "base" ΛCDM model the neutrino mass is fixed so that $\sum m_\nu = 0.06$eV, which is the lower bound allowed by oscillation experiments.

Here it is a commonly used combination of this six parameters:

1. the density parameter for cold dark matter Ω_c;
2. the density parameter for baryonic matter Ω_b [26] [16] [12];
3. the dimensionless current Hubble constant h;
4. the optical depth to reionization τ;

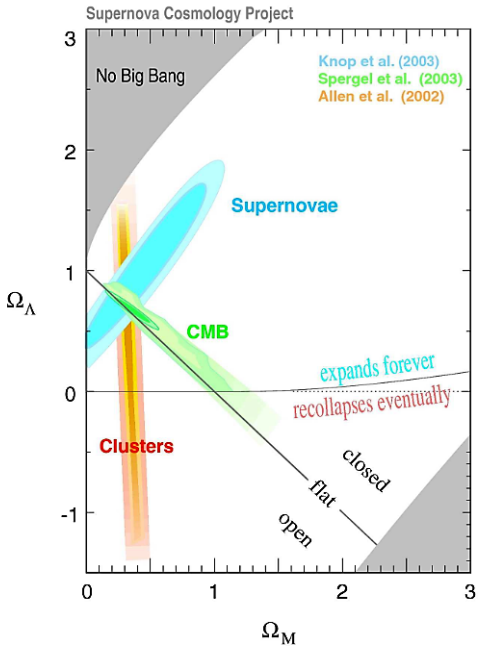

Figure 1.1: Combined constraints to cosmological densities Ω_Λ and $\Omega_M = \Omega_c + \Omega_b$ obtained from independent measurements using supernovae, CMB and cluster abundance data. The flat Universe with Ω_Λ and Ω_M is shown with solid line [21].

5. the amplitude A_s of the primordial power spectrum;

6. the spectral index n_s of the primordial power spectrum.

This base model, even though already successful, can be extended adding new parameters. In this dissertation we will particularly focus on a one-parameter extension called ΛCDM + $\sum m_\nu$ model [26] in which the seventh parameter is $\sum m_\nu$.

This extended model is interesting because it allows to analyse how much the cosmological data are able to bind the sum of neutrino masses. The presence of neutrinos modifies the evolution of the cosmological observables in peculiar ways. Therefore, by reconstructing how neutrinos have influenced the evolution, we can get some bounds about their properties, including their masses.

Chapter 2

Neutrino Cosmology

2.1 Short neutrino cosmic history

We have already seen in Sec.1.4 that neutrino equation of state parameter w is not constant. This is due to the fact that, during their evolution, neutrinos passed through different scenarios.

In this thesis we consider only light neutrinos (sub-eV), in agreement with current limits from theory and laboratory results (e.g. Planck [40] and Katrin [47] Experiment).

In the early Universe, neutrinos are ultra-relativistic and behave like radiation. They are kept in equilibrium with the cosmological plasma by weak interactions. This is true until when:

$$\Gamma_{int}(z) \gg H(z). \tag{2.1}$$

$\Gamma_{int}(z) = n\langle\sigma v\rangle$ is the interaction rate, with σ the cross-section, v the velocity of the particles and the angular brackets indicating a thermal average.

For neutrinos, we can take $v \approx c$, since we are in the ultra-relativistic limit, and $\sigma \propto G_F T_\nu^2$, with G_F the Fermi constant. Moreover, for a single neutrino species n, considering both neutrinos and antineutrinos, according to the Fermi-Dirac statistics, n_ν becomes:

$$n_\nu(T_\nu) = \frac{g}{(2\pi)^3}\int \frac{d^3\vec{p}}{e^{p/T_\nu}+1} = \frac{3\zeta(3)}{4\pi^2}T_\nu^3, \tag{2.2}$$

where ζ is the zeta Riemann function and $g = 2$ for neutrinos [26].

From (1.9), we get that the r.h.s. of (2.1) is $H^2(z) = (8\pi G/3)(\rho_\gamma + \rho_\nu)$, where, since we are in the early times of the Universe, we considered just the

radiative contributions to the energy density from photons and neutrinos. For the last ones, the energy density is:

$$\rho_\nu(T_\nu) = \frac{g}{(2\pi)^3}\int \frac{\sqrt{p^2+m_\nu^2}}{e^{p/T_\nu}+1}\, d^3\vec{p} = \begin{cases} \frac{7\pi^2 T_\nu^4}{120}, & \textit{ultra-relativistic} \\ m_\nu n_\nu, & \textit{non-relativistic} \end{cases} \tag{2.3}$$

Photon energy density $\rho_\gamma \propto T^4$, too. As we will see below, $T_\nu \propto T_\gamma$. Therefore, since we are in the RD era, from (1.4a) we obtain $H^2 \propto T^4$.

Substituting the first line of (2.3) in (2.1), we get that $\Gamma_{int}(z) \approx H(z)$ for $T_\nu \approx 1$ MeV. Once the Universe falls below this temperature, neutrinos decouple from the plasma.

Shortly after neutrino decoupling, $e^\pm$ annihilation starts and, as a consequence, photons reheat in order to conserve entropy. This reheating does not involve the neutrinos since they are no more in equilibrium with the plasma [27]. Eventually, we get the following relation between neutrino temperature T_ν and photon one T_γ:

$$T_\nu = \left(\frac{4}{11}\right)^{1/3} T_\gamma. \tag{2.4}$$

To get this relation, we have also taken into account that at the temperature $\mathcal{O}(MeV)$ neutrinos are still ultrarelativistic. Therefore, in agreement with the Liouville theorem, the shape of the distribution is preserved during the expansion so that neutrinos are described by the Fermi-Dirac statistics even when they become nonrelativistic [26].

Using (2.3) and (2.4), we can explicit the radiation contribution from photons and neutrinos to energy density during the RD era:

$$\rho_{\gamma+\nu} = \rho_\gamma\left[1+\frac{7}{8}\left(\frac{4}{11}\right)^{4/3} N_\nu\right], \tag{2.5}$$

where N_ν is the number of active neutrino species. In the framework of the SMPP $N_\nu = 3$.

However, (2.5) is valid only under the assumption of instantaneous neutrino decoupling. Actually, since neutrino decoupling and $e^\pm$ annihilation happen almost at the same temperature, there are some relic interactions between neutrinos and $e^\pm$. Therefore, in order to account for this effect and even of finite temperature QED radiative corrections and flavour oscillations [8], (2.5) becomes:

$$\rho_{\gamma+\nu} = \rho_\gamma\left[1+\frac{7}{8}\left(\frac{4}{11}\right)^{4/3} N_{eff}\right], \tag{2.6}$$

with $N_{eff} = 3.044$ [42].

Once neutrinos become nonrelativistic, they behave as matter.

According to (2.4), from CMB temperature measurements we can get the present time neutrino temperature. As a result, using (2.2) and (2.3) we get for the total density parameter of massive neutrinos Ω_ν a relation valid at late time depending only on $\sum m_\nu$:

$$\Omega_\nu h^2 = \frac{\sum m_\nu}{93.14\text{eV}}. \tag{2.7}$$

In the instantaneous neutrino decoupling approximation, the factor at the denominator is replaced by 94.2 eV.

2.2 Cosmological neutrino effects

Neutrino properties effects on cosmological evolution can be divided in two areas:

- *background effects* modifying the evolution of the FLRW metric;
- *perturbation effects* modifying the evolution of the perturbations in the gravitational potential and in the components of the cosmic fluid.

2.2.1 Background effects

Considering the ΛCDM+$\sum m_\nu$ model described at the end of Sec. 1.4, we can express the relation (1.9) in the form:

$$\omega_c + \omega_b + \omega_\nu + \omega_\Lambda + \omega_k = h^2. \tag{2.8}$$

In agreement with (2.7), increasing $\sum m_\nu$, we increase ω_ν. We start considering a reference model with $\sum m_\nu = 0.06eV$, the minimum allowed by oscillation experiments. According to our model, $\omega_k = 0$, while both ω_γ and ω_b are well known [43] [6]. Therefore, so that (2.8) remains valid while increasing $\sum m_\nu$, we have got three possibilities:

- *increasing h, keeping ω_c and ω_Λ constant*: looking at the equation (1.13), we see that the only varying term in the l.h.s. is the neutrino one. Indicating z_{nr} the redshift at which neutrinos become nonrelativistic, for $z \gg z_{nr}$, $h(z)$ does not change since ρ_ν in the ultrarelativistic limit does not vary with the mass. On the contrary, in the nonrelativistic limit ($z \lesssim z_{nr}$), $h(z)$ increases as m_ν;

- *lowering ω_c keeping h and ω_Λ constant*: looking at (1.13), we see that for low redshift, until $z < z_{nr}$, $h(z)$ is the same since the increase in m_ν is compensated by the decrease in ω_c. On the other hand, for $z > z_{nr}$ the neutrino density ρ_ν is the same as in the reference model, so that the decrease in ω_c results in lowering $h(z)$. This is true until the beginning of the RD era during which the matter contribution to energy density becomes negligible so that $h(z)$ is alike the reference model one;

- *lowering ω_Λ keeping h and ω_c constant*: since the cosmological constant term in (1.13) does not depend on the redshift, first of all lowering ω_Λ results in expanding the MD era. Moreover, while for $z > z_{nr}$ $h(z)$ is identical to the reference model because ω_Λ is negligible and $\sum m_\nu$ does not change with z, for $z < z_{nr}$ $h(z)$ decreases for lower values of ω_Λ.

To summarize, changes in $\sum m_\nu$ affect the transition epochs and the expansion rate.

2.2.2 Perturbation effects

Since we can observe experimentally perturbations in radiation and matter fields, let us analyse the effects on them separately (for a more accurate analysis look at [26] [27]).

Photon perturbations

The photon perturbations are influenced by time variations in the gravitational potentials along the line of sight between us and the last scattering surface, i.e. the surface at which photons stopped scattering at the end of the recombination epoch when electrons started recombining in atoms. This effect, called *integrated Sachs-Wolfe* (ISW) effect, is negligible in the MD era during which the gravitational potentials are almost constant, while is important early after the recombination (*early ISW*) in the RD era and late during the DE era (*late ISW*).

Therefore, delaying the matter-radiation equality or anticipating the DE era as a result of varing $\sum m_\nu$ would increase respectively the early ISW or late ISW contribution.

Matter perturbations

Even in this case, a first effect is related to the time of matter-radiation equality since the growth of the matter perturbations takes place mainly

during the MD era and, as we have seen above, the value of $\sum m_\nu$ can affect the lenght of this era.

Another effect involves the clustering properties of neutrinos. Relativistic neutrinos tend to *free stream* out from overdense regions damping all the small-scale neutrino density fluctuations below the horizon scale [27]. Neutrino clustering is suppressed below the so-called *free-streaming scale* defined as the horizon at the epoch of the transition from ultrarelativistic to non-relativistic neutrino regime. In the hypothesis of sub-eV neutrinos the transition happens during the MD era, so that we get the relation:

$$k_{fs} \simeq 0.018\ \Omega_m^{1/2} \left(\frac{m_\nu}{1eV} \right)^{1/2} \text{h Mpc}^{-1}, \tag{2.9}$$

where m_ν is one of the neutrino mass eigenstates, $\Omega_m = \Omega_b + \Omega_c + \Omega_\nu$ and h is the usual dimensionless Hubble parameter at the present time [26].

On the opposite, above the free-streaming scale, i.e. $k < k_{fs}$, neutrinos cluster as matter.

Looking at equation (2.9), we realize that increasing neutrino masses causes the growth of k_{fs} and, as a result, the suppression of neutrino fluctuations at small-scale. This slows down the growth of small-scale for other matter components, due to the fact that neutrinos do not contribute to the gravitational potential at those scales. It is like the small-scale perturbations evolved in a mixed radiation-matter Universe in which the growth of the perturbations is slower than in a pure matter one.

For this reason, neutrinos are a type of *hot dark matter* (HDM). In presence of HDM, cosmological structures evolve according to a *top-down* scenario, i.e. large objects like clusters form first, than smaller ones form via a fragmentation process. This scenario is not in agreement with observations according to which small structures seem older than larger ones (*bottom-up* scenario, typical of CDM). Historically this led to exclude neutrinos as DM candidates.

Chapter 3

The matter power spectrum

In section 1.3 we have already introduced cosmological perturbations. The local deviations from average density induce local differences in gravity, so that where the density is higher, the gravitational force is larger. The opposite happens in regions with lower density.

The overdensities result in attracting more and more matter until when these regions decouple from the Hubble-Lemaître expansion starting to collapse forming gravitationally bound objects.

This is the commonly accepted scenario describing the structure formation.

As a consequence, it is really important to study the local density contrast

$$\delta(\vec{x}, z) = \frac{\rho(\vec{x}, z) - \rho_u(z)}{\rho_u(z)}, \tag{3.1}$$

where $\rho_u(z)$ is the background uniform density and z is the redshift at which the density is evaluated. In this definition, we used the comoving coordinate $\vec{x}$:

$$\vec{x}(t) = \frac{\vec{r}(t)}{a(t)}, \tag{3.2}$$

with $\vec{r}(t)$ the physical position of the object and $a(t)$ the scale factor.

In term of (3.2) we can also define the comoving causal horizon:

$$r_h(t) = \int_0^t \frac{dt'}{a(t')} = \int_z^\infty \frac{dz'}{H(z')}, \tag{3.3}$$

representing the distance travelled by a photon from the Big-Bang ($t = 0$ or $z = \infty$) until the time t (corresponding redshift z).

3.1 Two-point correlation function

The two-point correlation function is defined as the ensemble average[1] of the density contrast at two different positions [9]:

$$\xi(r,z) = \langle \delta(\vec{x},z)\delta(\vec{x}+\vec{r},z)\rangle. \tag{3.4}$$

Assuming the cosmological principle 1.1, ξ depends just on the norm of $\vec{r}$. In fact, the homogeneity and isotropy at large scale imply respectively that ξ is invariant for translation of $\vec{x}$ and $\vec{x}+\vec{r}$ and for spatial rotation.

3.2 Power Spectrum

3.2.1 Linear Perturbation Theory

According to homogeneity and isotropy hypothesis, we can describe the cosmological background as a perfect pressureless fluid. Since the structure formation involves matter which is mainly nonrelativistic in the ΛCDM model, the equations describing the cosmological background and the density contrast $\delta(\vec{x},z)$ are the Newtonian ones, i.e. the continuity, Euler and Poisson equations. In particular, for the density contrast we get [33] [50]:

1. the *Continuity Equation* describing the conservation of the mass:

$$\frac{\partial\delta(\vec{x},\eta)}{\partial\eta} + \vec{\nabla}\cdot[(1+\delta(\vec{x},\eta))\vec{v}(\vec{x},\eta)]; \tag{3.5}$$

2. the *Euler equation* describing the conservation of the momentum:

$$\left[\frac{\partial}{\partial\eta} + \vec{v}(\vec{x},\eta)\cdot\vec{\nabla}\right]\vec{v}(\vec{x},\eta) = -\frac{da}{d\eta}\frac{\vec{v}(\vec{x},\eta)}{a} - \vec{\nabla}\Phi; \tag{3.6}$$

3. the *Poisson equation* relating the gravitational potential to its source:

$$\nabla^2\Phi = 4\pi G a^2 \rho_u \delta(\vec{x},\eta), \tag{3.7}$$

[1] Here and after the angular brackets $\langle\cdots\rangle$ indicate an *ensemble average*. We have seen that the density contrasts result as fluctuations from an homogeneous background. Therefore, statistical information about them can be obtained averaging over all the possible realizations. Obviously, we have not access to different realizations of our Universe. However, thanks to the homogeneity and isotropy hypothesis (see Sec. 1.1), instead of an ensemble average we can do an average over limited portions of the Universe that are widely separated so that they can be assumed as statistically independent. This is also called *ergodic hypothesis* [23].

where Φ is the gravitational potential, $\vec{v} = d\vec{x}/d\eta$ is the velocity field and η is the *conformal time*. The conformal time is defined as the comoving distance that light can travel in a time interval [19] In other terms, we get:

$$d\eta = \frac{dt}{a(t)}. \tag{3.8}$$

Assuming small fluctuations [9], we can linearize the equations (3.5), (3.6), (3.7) and solve them in the Fourier space [2]: in this way, the above differential equations become algebraic equations [50] which are easier to be solved and whose solution we indicate as $\delta^{(1)}(\vec{k}, z)$, where the time dependence is expressed in term of the redshift z. Moreover, in the linear regime each Fourier mode evolve independently conserving the primordial statistics [9].

3.2.2 Power Spectrum

We can define:

$$\begin{aligned}\langle \delta^{(1)}(\vec{k}, z)\delta^{(1)}(\vec{k'}, z)\rangle &= \int d^3\vec{x}\; d^3\vec{r}\; \langle \delta^{(1)}(\vec{x}, z)\delta^{(1)}(\vec{x}+\vec{r}, z)\rangle\; e^{-i(\vec{k}+\vec{k'})\cdot\vec{x}}\; e^{-i\vec{k}\cdot\vec{r}} = \\ &= (2\pi)^3\delta_D(\vec{k}+\vec{k'}) \int d^3\vec{r}\; \xi^{(1)}(r, z)\; e^{i\vec{k}\cdot\vec{r}} = \\ &= (2\pi)^3\delta_D(\vec{k}+\vec{k'})P(k, z).\end{aligned} \tag{3.9}$$

$P(k)$ is by definition the matter power spectrum. In other words, we can define the power spectrum as the Fourier transformed two-point correlation function:

$$P(k, z) = \int d^3\vec{x}\; \xi^{(1)}(r, z)e^{-i\vec{k}\cdot\vec{x}}, \tag{3.10}$$

where $\xi^{(1)}(r, z)$ is the first order approximation for the two-point correlation function.

Considering the density contrast for non-relativistic matter, we talk about matter power spectrum $P_m(k)$ [27].

[2] We Fourier transform according to the following convention:

$$\delta(\vec{k}, z) = \int d^3\vec{x}\; \delta(\vec{x}, z)e^{-i\vec{k}\cdot\vec{x}}.$$

3.2.3 Primordial Power Spectrum

According to the inflation hypothesis, the first perturbations went through an exponential expansion. It can be shown that in the simplest inflation scenarios, the power spectrum of primordial scalar perturbations is $P_0(k)$ (see [5] and references therein):

$$P_0(k) \propto A_s k^{n_s - 1}. \tag{3.11}$$

The amplitude A_s and the spectral index n_s, as seen in Sec. 1.4, can be used as cosmological parameters.

The primordial power spectrum is modified during the evolution of the Universe. In particular, all the scales entering the horizon at a certain epoch are evolved, while the scales larger than the horizon do not change.

3.3 The evolution of the matter power spectrum

At this point, it is useful to briefly review the evolution of the matter power spectrum and its dependence on redshift. Following the Ref. [28], we will obtain our results in term of *a* which is related to *z* according to the relation $a = (1 + z)^{-1}$.

We consider only perturbations of CDM: we take this choice to keep things simple and because CDM is the principal matter component. Combining the Eqs. (3.5) and (3.6) in the Fourier space we obtain the equation of evolution for δ_c:

$$\frac{\partial^2 \delta_c}{\partial \eta^2} + \frac{1}{a}\frac{\partial}{\partial \eta}\frac{\partial \delta_c}{\partial \eta} = -k^2\psi + 3\frac{\partial^2 \Phi}{\partial \eta^2} + \frac{3}{a}\frac{\partial a}{\partial \eta}\frac{\partial \Phi}{\partial \eta}, \tag{3.12}$$

where Φ is the Newtonian potential and ψ the spatial curvature we find in the Einstein-Boltzmann equations we talked about in Sec. 1.3.

The Eq. (3.12) has different solutions according to the *k*'s scale:

1. for scales larger than the horizon, δ_c evolves with *a* depending on the dominant energy density component (e.g. during the RD era $\delta_c \propto a^2$);
2. for scales entering the horizon, i.e. becoming smaller than the horizon, during the RD era δ_c evolves in two stages:
   (a) until the end of the RD era, the perturbations do not grow (we talk about *stagnation* or *freezing-in* of matter perturbations [53]);
   (b) starting the MD era, perturbations evolve with $\delta_c \propto a$;
3. for scales entering the horizon during the MD era $\delta_c \propto a$.

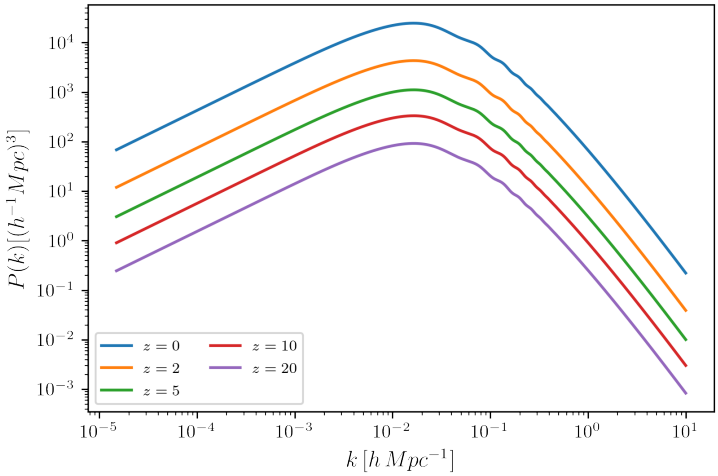

Figure 3.1: Matter power spectrum for different values of z.

Once we obtain δ_c, we can calculate the matter power spectrum:

$$P_m(k,a) = \left[\frac{aD(a)}{a_0}\right]^2 \frac{kP_0(k)}{\left(\Omega_m a_0^2 H_0^2\right)^2} \cdot \begin{cases} \frac{8\pi^2}{25}, & a_0 H_0 < k < k_{eq} \\ \frac{k_{eq}^4}{2k^4}\left(\alpha + \beta \ln\left(\frac{k}{k_{eq}}\right)\right)^2, & k > k_{eq} \end{cases} \tag{3.13}$$

with α and β numerical coefficients independent of k and

$$k_{eq} = a_{eq} H_{eq}, \tag{3.14}$$

where a_{eq} and H_{eq} are respectively the scale factor and the Hubble-Lemaître constant at the time of the equivalence matter-radiation, i.e. the epoch at which the transition from the RD era to the MD era happens.

$D(a)$ is the growth factor defined as:

$$D(a) = \frac{a_m \delta_c(k,a)}{a \delta_c(k,a_m)}, \tag{3.15}$$

where a_m is the scale factor at some time deep inside the MD era.

The combination of the three above solutions for the perturbations evolution causes the shape of the matter power spectrum.
The scales before the turning point were larger than the horizon at z_{eq} and, as a consequence, do not differ from the primordial matter power spectrum. The scales after the turning point were smaller than the horizon at z_{eq}. Therefore, they change with the cosmic evolution according to what we said above at the points 2 and 3.

To sum up, we can rewrite the Eq. (3.13) as:

$$P(k,a) = \left[T(k,a)\right]^2 P_0(k). \tag{3.16}$$

Parameter	Value
ω_b	0.02242
ω_c	0.11933
τ	0.0561
A_s	2.105×10^{-9}
n_s	0.9665
h	0.6766
$\sum m_\nu$	$0.06\ eV$
N_{eff}	3.046

Table 3.1: Reference Cosmological Parameters

$T(k, a)$ is called *transfer function*. It tell us how the primordial matter power spectrum has been modified by the evolution in order to obtain the matter power spectrum at a given redshift.
In Fig. 3.1 we can see how the matter power spectrum changes with z.

To study the matter power spectrum $P_m(k)$, we can use the Boltzmann codes calculating theoretical power spectra given a set of cosmological parameters. In the present work, we will use the Boltzmann code CAMB [2].

To sum up: $P_m(k)$ gives us a lot of information about the cosmic evolution and the various cosmological parameters. It is important to underline that we can measure $P_m(k)$ at different z and get informations about the Universe at that epochs.

From large scale, i.e. small k's, we can extrapolate information about the primordial fluctuations during inflation. On the other hand, smaller scales underline what happens when a fluctuation enters the horizon. This aspect is particular interesting because, as we have already said in Sec. 2.2.2, the perturbations grow faster during the MD era, so that we see a turning point in the power spectrum corresponding to the horizon at z_{eq}, as reported in Fig.3.2 in which we use the parameters from the Planck collaboration 2018 [6] in Table and, in agreement with our ΛCDM + $\sum m_\nu$ we have also considered a reference mass value $\sum m_\nu = 0.06\ eV$ and $N_{eff} = 3.046$ [3] (see Table 3.1)[4] [42] [20] [37] [8].

On the contrary, fluctuations grow slower during DE era, so that anticipating the matter-dark energy transition z_Λ will suppress the power spectrum. Moreover, looking at the equation (3.3), we can see that increasing

[3] In the present work, instead of the more precise value 3.044, we will use 3.046 in agreement with Planck 18 and we are not enough sensitive respect to the difference between them.

[4] All the figures in this chapter are realized taking the redshift $z = 0$ and the parameter from Table 3.1

[5] This and the following figures are produced using CAMB via Python programming.

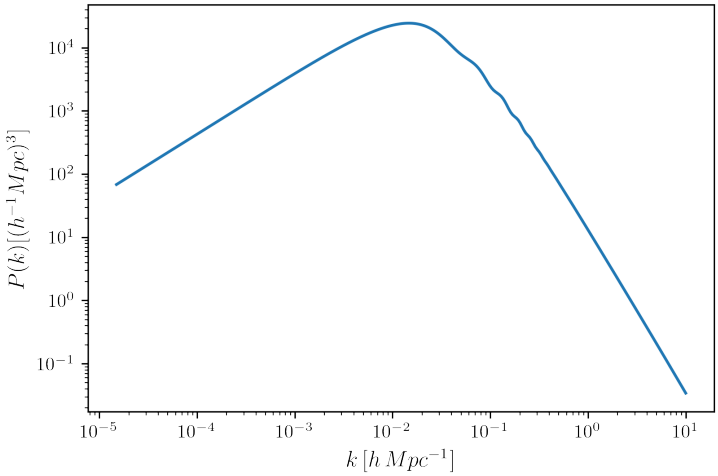

Figure 3.2: Matter power spectrum at $z = 0$ [5]

h will result in lowering r_h and, consequently, increasing the value of the k modes which can enter the horizon (see Fig. 3.3).

In the right side of the matter power spectra, after the turning point, we can see also an oscillatory trend. This is due to the so called *baryon-acoustic oscillations* (BAO): these are the acoustic oscillations in the photon-baryon fluid that remain frozen when baryon decouple from photons. Even though, after recombinations, photons decouple from the matter, the huge photons-to-baryons ratio of $\mathcal{O}(10^{10})$ [6] still keeps for a while the baryons coupled to the photon bath [26].

We have already seen the neutrino impact on the evolution of matter perturbations in Ch.2. In the next section we will see how the matter power spectrum changes when varying $\sum m_\nu$.

For a fuller description about the evolution of the matter perturbations in a Universe with mixed matter components (i.e. CDM and baryonic matter) the interested reader is referred to Ref. [27] [29].

3.4 Neutrino effects on the matter power spectrum

As we have said in Sec. 2.2, neutrino masses can influence the cosmological evolution and, therefore, the matter power spectrum, too.

Firstly, we analyse the case in which the increase of $\sum m_\nu$ is compensated by increasing h^2 (see Fig.3.4). It is relevant comparing the figures 3.3

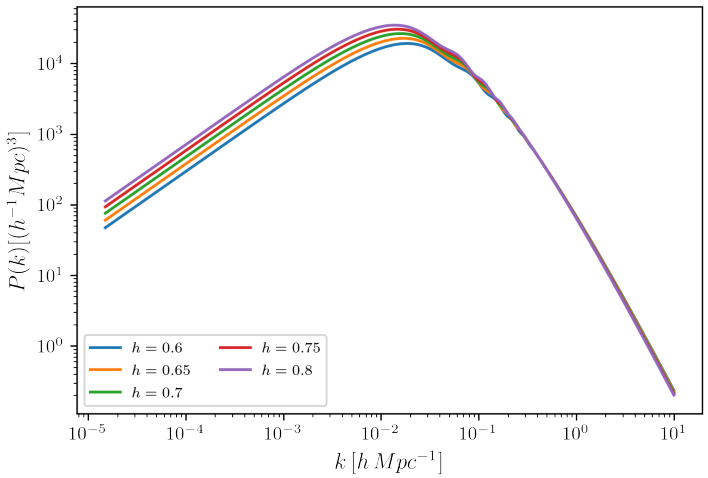

Figure 3.3: Matter power spectrum for different values of h: increasing h corresponds to increasing all the power spectrum.

and 3.4: in both cases h is increasing, but we see a different behaviour in the spectra.

In both cases, in the left side we see the spectra increasing with h. This is no more true in the right side: in 3.4 the spectra are suppressed for increasing h. This is due to the fact that in this case we are varying not only h, but even $\sum m_\nu$ whose growth, as seen in 2.2.2, suppresses clustering at small scale.

We understand that varying two o more parameters allows to decrease background effects lightening up the perturbations ones and allowing to constrain cosmological parameters. This is what we will do this in the next chapters.

Another interesting case is the one in which the increasing neutrino mass is compensated by lowering ω_c keeping $\omega_c + \omega_\nu$ and all the other cosmological parameter constant.

From Fig.3.5 it is evident that the matter power spectra at small k's do not show any difference. This is due to the fact that, for $k < k_{fs}$ neutrinos can cluster behaving as cold dark matter.

On the other hand, as underlined in the Sec. 2.2.2, the neutrino clustering for $k > k_{fs}$ are suppressed and even the growth of other matter component perturbations. As a consequence, increasing $\sum m_\nu$ will get $P_m(k)$ down.

For the sake of better understanding this asymptotic behaviour, we in-

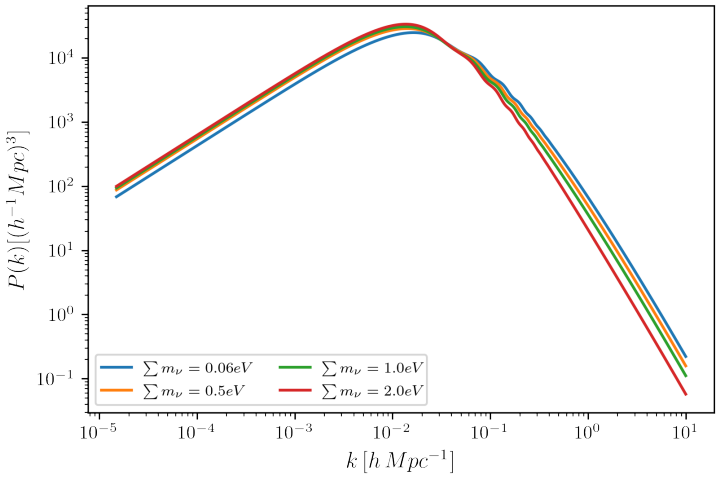

Figure 3.4: Matter power spectrum for increasing $\sum m_\nu$: the growth of $\sum m_\nu$ is compensated by the growth of h.

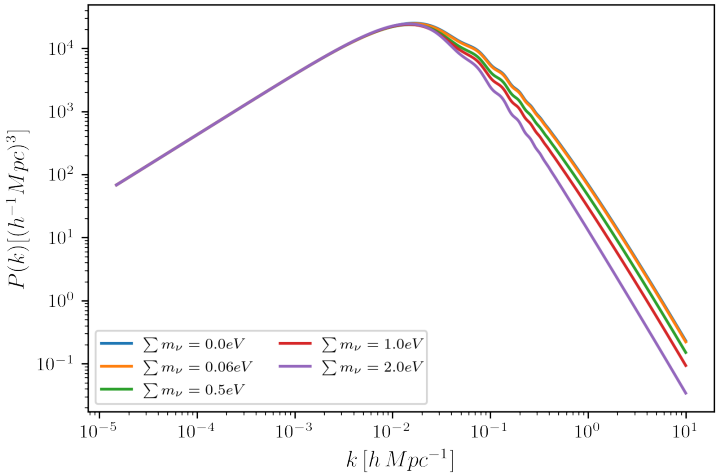

Figure 3.5: Matter power spectrum for different values of ω_c and ω_ν keeping $\omega_c + \omega_\nu$ constant.

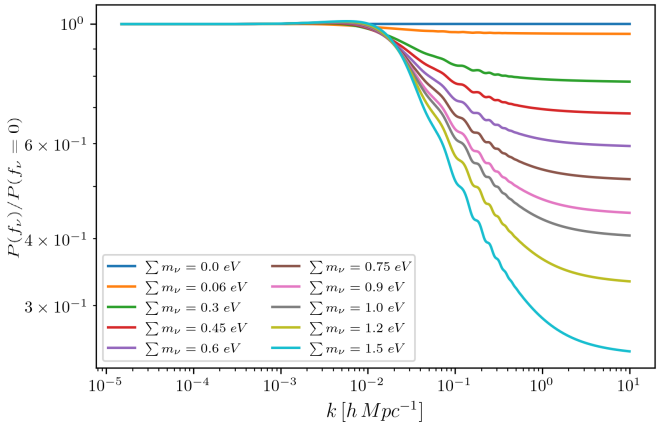

Figure 3.6: Ratio of massive neutrinos matter power spectrum to massless neutrinos power spectrum: for the former, we vary ω_c and ω_ν keeping $\omega_c + \omega_\nu$ constant.

troduce the approximation at $z = 0$ [26]:

$$\frac{P_m(k \gg k_{fs}, f_\nu)}{P_m(k \gg k_{fs}, f_\nu = 0)} \simeq 1 - 8f_\nu, \tag{3.17}$$

with $f_\nu = \Omega_\nu/\Omega_m$, valid until when $f_\nu < 0.07$ [27]. Applying it to the same configuration used in Fig. 3.5 we get the results in 3.6, where we can see the curves reaching a plateau between $k = 1$h Mpc^{-1} and $k = 10$h Mpc^{-1}

In order to verify the validity of (3.17), we plot f_ν against the ratio $P(f_\nu)/P(f_\nu = 0)$ evaluated at $k = 10$h Mpcc^{-1} for all the different values of $\sum m_\nu$. From Fig. 3.7, we get that, as expected, the approximation looses validity for $f_\nu > 0.07$.

3.5 Non-linear Matter Power Spectrum

So far, we have considered small fluctuations with respect to the background (i.e. $\delta_m \ll 1$), so that we have been able to limit ourself just to the linear theory in solving the fluid equations 3.5, 3.6 and 3.7.

Actually, at each redshift z there's a scales k_{nl} below which $\delta_m \sim 1$. In this case, the linear theory does not well describe the cosmic evolution. We have to introduce a non-linear study and define the *non-linear matter power spectrum* P_{nl}:

$$\langle \delta(\vec{k}, z)\delta(\vec{k'}, z)\rangle = (2\pi)^3 \delta_D(\vec{k} + \vec{k'})P_{nl}(k, z). \tag{3.18}$$

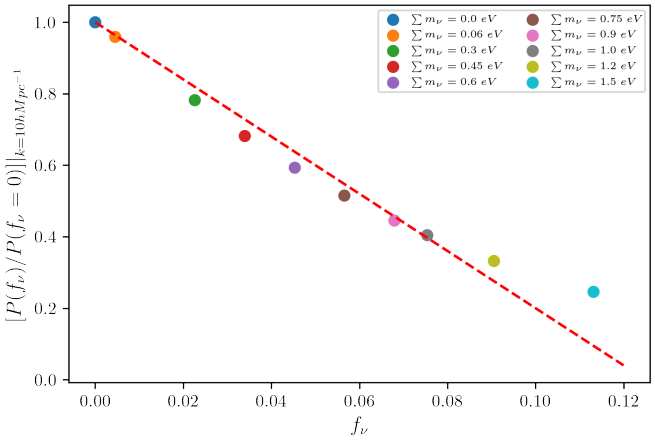

Figure 3.7: Ratio of massive neutrinos matter power spectrum to massless neutrinos power spectrum as a function of f_ν. The red dashed line shows the expected trend $(1 - 8f_\nu)$.

Looking at Fig.3.8 we can see that at large scales, the non-linear power spectrum coincide with the linear one, while this is not true at small scales: the former is bigger due to the growing contributions from non-linearities. In other words, in the ΛCDM model we see a hierarchical structure formation, with smaller scale going non-linear earlier [5].

The study of $P_{nl}(k, z)$ is complex: it can be done using, for instance, N-body simulations like the MassiveNus simulations [34] which have to take into account the astrophysical and hydrodynamical processes happening at these scales [26].

Despite this complexity, the non-linear study is really useful. First of all, we could extract much more information from a survey dataset if we extend the comparison between theory and data to smaller scales, under the condition that the theoretical uncertainties are smaller than the instrumental ones [5].

Moreover, as we will see in the next chapter, the non-linear treatment allows to get informations about the distribution of matter on large scales that we are not able to achieve with direct observations due to experimental limits.

3.5.1 Neutrino effects on $P_{nl}(k, z)$

It is interesting analysing the neutrino effects on the non-linear matter power spectrum studying the ratio $P_{nl}(f_\nu)/P_{nl}(f_\nu = 0)$, as done in the last part of

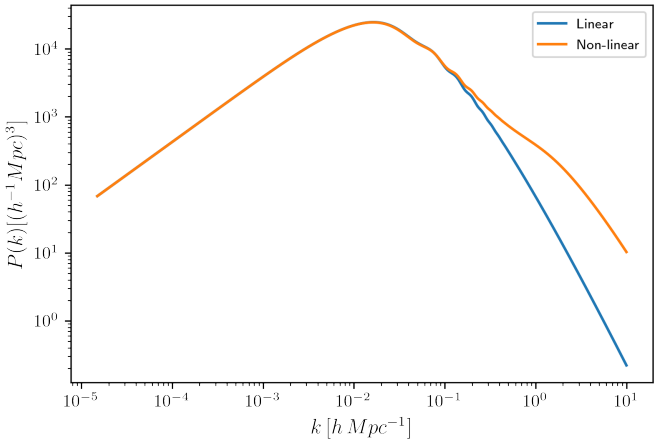

Figure 3.8: Linear and non linear power spectrum

the Sec. 3.4.

Using the same parameters configuration as in Fig. 3.6, we get the Fig. 3.9.

In Fig. 3.10 we can compare the two different cases: until $k \sim \mathcal{O}(10^{-1}\text{h Mpc}^{-1})$ the curves are almost the same for both cases. Then, the non-linear curves fall down until a minimum at $k_{min} \sim \mathcal{O}(1\text{h Mpc}^{-1})$ and, later, start increasing describing a spoon shape [29].

For the minimum of the spoon shape curves, we can express a similar formulation of 3.17:

$$\frac{P_{nl}(k_{min}, f_\nu)}{P_{nl}(k_{min}, f_\nu = 0)} \simeq 1 - 10 f_\nu. \tag{3.19}$$

Plotting the ratio $P(f_\nu)/P(f_\nu = 0)$ evaluated at $k = 1\text{h Mpc}^{-1}$ against f_ν for all the different value of $\sum m_\nu$, we can see that, as expected, the relation $(1 - 10 f_\nu)$ describes the trend better than $(1 - 8 f_\nu)$. Even in this case, the approximation seems loosing validity for $f_\nu > 0.07$.

The spoon shape is the result of the combination of two effects [29]:

1. as we have said in Sec.2.2.2, increasing $\sum m_\nu$ results in slowing the growth of structure at small scale. Therefore, they enter later into the non-linear regime adding a suppression effect to the linear one. This explains the slower trend $(1 - 10 f_\nu)$ instead of $(1 - 8 f_\nu)$;

2. in the non-linear regime, the matter power spectrum looses memory of its initial conditions, so that for large k the ratio between massive neutrino spectrum and massless one should be asymptotically one.

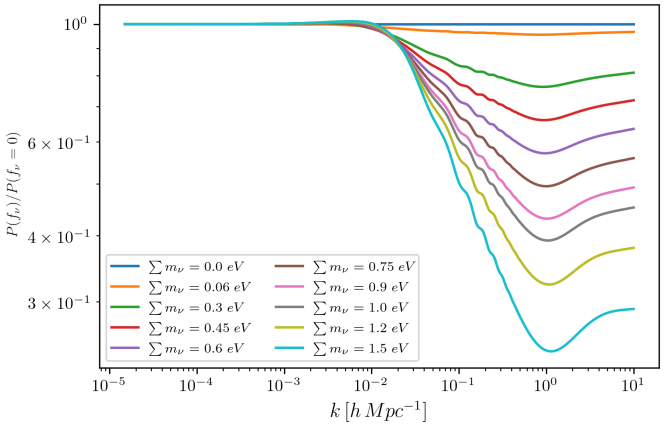

Figure 3.9: For all the spectra, $\omega_c + \omega_\nu$ and all the other cosmological parameters are constant.

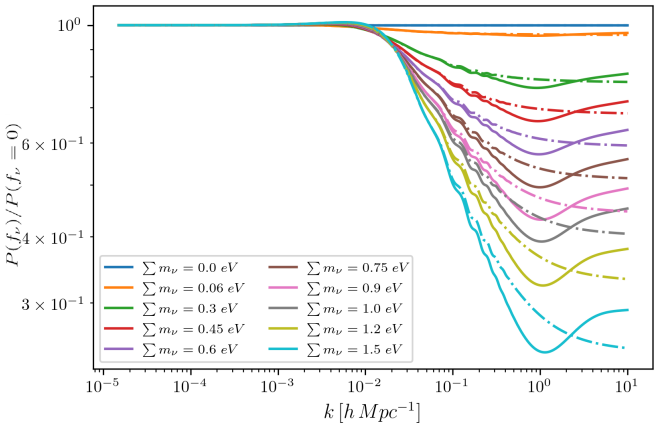

Figure 3.10: Ratio of massive neutrinos matter power spectrum to massless neutrinos power spectrum: for the former, we vary ω_c and ω_ν keeping $\omega_c + \omega_\nu$ constant. The solid lines are used for the non-linear spectra while the dashed ones for the linear ones.

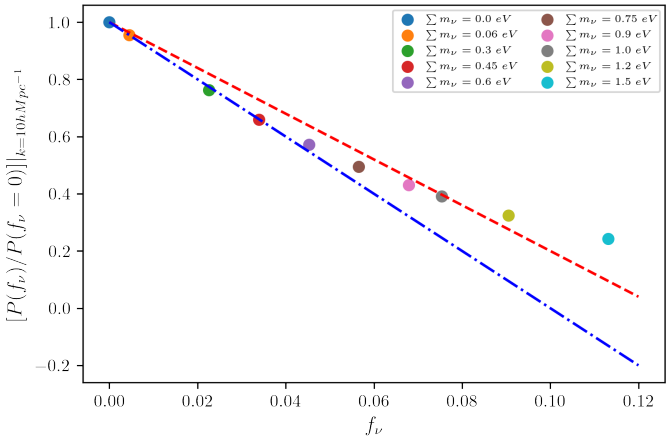

Figure 3.11: Ratio of massive neutrinos matter power spectrum to massless neutrinos power spectrum as a function of f_ν. The solid lines are used for the non-linear spectra while the dashed ones for the linear ones.The blue dot dash line shows the trend $(1 - 10f_\nu)$ while the red dashed one shows the trend $(1 - 8f_\nu)$.

3.6 Galaxy Power Spectrum

Galaxy surveys allow to measure $3D$ spatial distribution of galaxies and to achieve the power spectrum of galaxies $P_g(k, z)$. Actually, surveys are sensitive just to luminous matter, so that galaxy power spectrum $P_g(k, z)$ can differ from $P_m(k, z)$: galaxies are defined as a *biased tracer* of matter distribution [26].

In order to take into account of this, we introduce the bias function $b(k, z)$, so that:

$$P_g(k, z) = b^2(k, z)P_m(k, z).^6 \tag{3.20}$$

The bias is scale and redshift dependent. Actually, at large scale it can be considered scale independent, while concerning the redshift dependence we can assume a simple redshift relation:

$$b(z) = b_0(1 + z), \tag{3.21}$$

where b_0 is the present time value.

Since the primary scope of this thesis is to develop a simple pipeline analysis to conduct exploratory studies on the impact of large-scale data, here we make some simplifying choices.

First, as already said, we neglect the scale dependence of the bias and assume a simple redshift dependence as in Eq. (3.21).

[6] This relation is valid both for linear and non-linear power spectrum

Secondly, in writing Eq. (3.20), we assume that P_g is related to the total matter power spectrum. However, it has been shown that Eq. (3.20) should have the power spectrum of cold and baryonic matter at the r.h.s. instead of the total P_m [7] [14] [35] [36].

Finally, we neglect the effect of redshift-space distortions, i.e., the fact that the use of the redshift as an indicator of the distance can induce distortions in the reconstructed maps of objects (see e.g. [23]).

Given the range of scales and redshifts considered in this work, the first and the second assumption are not too strong. The third assumption has been made to simplify our analysis, and will be eliminated in future works following Ref. [32].

Chapter 4

Large Scale Structure Reconstruction

As already said in Sec.3.5, measuring the distribution of matter on large scale is difficult due to experimental limits. For example, we should observe really large volumes and portions of sky detectable only via satellite. Furthermore, concerning the 21cm intensity mapping, it will be hard to measure large scale modes on the line of sight will never be measured directly because of the foregrounds [38].

However, we can reconstruct large scales indirectly studying how large scale overdensities modify the growth of small scale structures, in other words relating the linear matter power spectrum with the non-linear one[1]. In the present dissertation, we will follow the works by Li et al. (2020) [33] [32].

In order to achieve the reconstruction goal, it is useful starting reviewing the standard perturbation theory (SPT) up to second order.

4.1 Standard perturbation theory

The fluid equations (3.5), (3.6), (3.7) can be solved perturbatively in the Fourier space obtaining:

$$\delta(\vec{k},z)=\sum_{n=1}^{\infty}\delta^{(n)}(\vec{k},z)=\sum_{n=1}^{\infty}D_1^n(z)\delta^{(n)}(\vec{k}), \tag{4.1}$$

$$\theta(\vec{k},z)=\sum_{n=1}^{\infty}\theta^{(n)}(\vec{k},z)=-\frac{d\ln D_1(z)}{dz}\sum_{n=1}^{\infty}D_1^n(z)\theta^{(n)}(\vec{k}), \tag{4.2}$$

[1]Here and after we will indicate the matter power spectrum as linear matter power spectrum $P_{lin}(k,z)$.

where $\theta(\vec{k}, z)$ is the Fourier transform of $\vec{\nabla} \cdot \vec{v}(\vec{k}, z)$ and we isolate the time dependency in the so-called *linear growth factor* $D_1(z)$ [9].

The first term $\delta^{(1)}(\vec{k}, z)$ of the expansion (4.1) refers to the linear evolution, so that:

$$\langle \delta^{(1)}(\vec{k}, z)\delta^{(1)}(\vec{k'}, z)\rangle = (2\pi)^3 \delta_D(\vec{k} + \vec{k'})P_{lin}(k, z). \tag{4.3}$$

Substituting (4.1) and (4.2) in the Fourier transformed equations (3.5), (3.6), (3.7) we get for the second order term of (4.1) [33]:

$$\delta^{(2)}(\vec{k}, z) = \int \frac{d^3\vec{k}_1}{(2\pi)^3} F_2(\vec{k}_1, \vec{k} - \vec{k}_1)\delta^{(1)}(\vec{k}_1, z)\delta^{(1)}(\vec{k} - \vec{k}_1, z), \tag{4.4}$$

where[2]:

$$F_2(\vec{k_1}, \vec{k_2}) = \frac{5}{7} + \frac{2}{7}\frac{(\vec{k_1} \cdot \vec{k_2})^2}{k_1^2 k_2^2} + \frac{\vec{k_1} \cdot \vec{k_2}}{2k_1 k_2}\left[\frac{k_1}{k_2} + \frac{k_2}{k_1}\right]. \tag{4.5}$$

is symmetric under the exchange of its arguments.

As we will see in following equations, in these first steps into the study of the large scale structure reconstruction we will neglect the z dependence.

For the sake of relating large scale structures with small scale ones, it is useful to calculate the Fourier transformed two-point correlation function for two modes $\vec{k}_s$ and $\vec{k}'_s$ at small scale in the *squeezed limit* $\vec{k}_l = \vec{k}_s + \vec{k}'_s$, with $k_s, k'_s \gg k_l$ and $\vec{k}_l$ a large scale mode. To second order:

$$\begin{aligned}\langle \delta(\vec{k}_s)\delta(\vec{k}'_s)\rangle|_{\vec{k}_l = \vec{k}_s + \vec{k}'_s} &= \langle \delta^{(1)}(\vec{k}_s)\delta^{(2)}(\vec{k}'_s)\rangle + \langle \delta^{(2)}(\vec{k}_s)\delta^{(1)}(\vec{k}'_s)\rangle = \\ &= \langle \delta^{(1)}(\vec{k}_s)\delta^{(2)}(\vec{k}_l - \vec{k}_s)\rangle + \langle \delta^{(2)}(\vec{k}_s)\delta^{(1)}(\vec{k}_l - \vec{k}_s)\rangle.\end{aligned} \tag{4.6}$$

In the last equality we rewrite all the dependencies in term of $\vec{k}_s$ and $\vec{k}_l$.

For each term in the r.h.s. of (4.6), substituting the expression (4.4) for $\delta^{(2)}$, we get:

$$\langle \delta^{(1)}(\vec{k}_s)\delta^{(2)}(\vec{k}_l - \vec{k}_s)\rangle = \int \frac{d^3\vec{k}}{(2\pi)^3} F_2(\vec{k}, \vec{k}_l - \vec{k}_s - \vec{k})\langle \delta^{(1)}(\vec{k}_s)\delta^{(1)}(\vec{k}_l - \vec{k}_s - \vec{k})\delta^{(1)}(\vec{k})\rangle. \tag{4.7}$$

Since the small scale modes (large magnitude k) evolve independently of the large scale modes, we can take the large scale mode out of the 3-point

[2] Actually, (4.1), (4.2), (4.5) are exact just for a pressureless perfect fluid in an Einstein-de Sitter Universe, i.e. a flat matter dominated universe; however, the differences with the ΛCDM model are found to be negligible [48].

correlation function, so that:

$$\langle\delta^{(1)}(\vec{k}_s)\delta^{(1)}(\vec{k}_l-\vec{k}_s-\vec{k})\rangle\delta^{(1)}(\vec{k}) = \langle\delta^{(1)}(\vec{k}_s)\delta^{(1)}(\vec{k}_l-\vec{k}_s-\vec{k})\delta^{(1)}(\vec{k})\rangle + \\ + \langle\delta^{(1)}(\vec{k}_s)\delta^{(1)}(\vec{k})\rangle\delta^{(1)}(\vec{k}_l-\vec{k}_s-\vec{k}), \tag{4.8}$$

where the first term in the r.h.s. refers to the case with small $|\vec{k}|$ and second one to the case with small $|\vec{k}_l-\vec{k}_s-\vec{k}|$. Using the definition (4.3):

$$\langle\delta^{(1)}(\vec{k}_s)\delta^{(1)}(\vec{k}_l-\vec{k}_s-\vec{k})\delta^{(1)}(\vec{k})\rangle = (2\pi)^3 P_{lin}(k_s)\big[\delta_D(\vec{k}_l-\vec{k})\delta^{(1)}(\vec{k}) + \\ + \delta_D(\vec{k}_s+\vec{k})\delta^{(1)}(\vec{k}_l-\vec{k}_s-\vec{k})\big]. \tag{4.9}$$

Therefore, (4.7) becomes:

$$\langle\delta^{(1)}(\vec{k}_s)\delta^{(2)}(\vec{k}_l-\vec{k}_s)\rangle = P_{lin}(k_s)\int d^3\vec{k}\; F_2(\vec{k},\vec{k}_l-\vec{k}_s-\vec{k})\big[\delta_D(\vec{k}_l-\vec{k})\delta^{(1)}(\vec{k}) + \\ + \delta_D(\vec{k}_s+\vec{k})\delta^{(1)}(\vec{k}_l-\vec{k}_s-\vec{k})\big] = 2F(-\vec{k}_s,\vec{k}_l)P_{lin}(k_s)\delta^{(1)}(\vec{k}_l), \tag{4.10}$$

where in the last equality we use the symmetry of F_2.

Finally, we get to the second order:

$$\langle\delta(\vec{k}_s)\delta(\vec{k}_l-\vec{k}_s)\rangle = f(\vec{k}_s,\vec{k}_l-\vec{k}_s)\delta^{(1)}(\vec{k}_l), \tag{4.11}$$

where:

$$f(\vec{k}_s,\vec{k}_l-\vec{k}_s) = 2F_2(-\vec{k}_s,\vec{k}_l)P_{lin}(k_s)+2F_2(-\vec{k}_l+\vec{k}_s,\vec{k}_l)P_{lin}(k_l-k_s). \tag{4.12}$$

Looking at the above equations (4.11) and (4.12), we can deduct that it is possible to estimate large scale modes using small scale ones.

4.2 Quadratic estimator

Using the knowledge from the relation (4.11), we can formulate an estimator for large-scale modes. We start summing over as many pairs as possible with a weight function $g(\vec{k}_s,\vec{k}_l-\vec{k}_s)$:

$$\hat{\delta}^{(1)}(\vec{k}_l) = A(\vec{k}_l)\int\frac{d^3\vec{k}_s}{(2\pi)^3}g(\vec{k}_s,\vec{k}_l-\vec{k}_s)\delta(\vec{k}_s)\delta(\vec{k}_l-\vec{k}_s), \tag{4.13}$$

where:

$$A(\vec{k}_l) = \left[\int\frac{d^3\vec{k}_s}{(2\pi)^3}g(\vec{k}_s,\vec{k}_l-\vec{k}_s)f(\vec{k}_s,\vec{k}_l-\vec{k}_s)\right]^{-1} \tag{4.14}$$

is the normalization factor obtained requiring that $\langle\hat{\delta}^{(1)}(\vec{k}_l)\rangle = \delta^{(1)}(\vec{k}_l)$. Therefore, we get:

$$\begin{aligned}\langle\hat{\delta}^{(1)}(\vec{k}_l)\hat{\delta}^{(1)*}(\vec{k}'_l)\rangle &= (2\pi)^3\delta_D(\vec{k}_l-\vec{k}'_l)\big[P_{lin}(k_l)+N(\vec{k}_l)\big] = \\ &= (2\pi)^3\delta_D(\vec{k}_l-\vec{k}'_l)\big[P_{nl}(k_l)+N(\vec{k}_l)\big],\end{aligned} \tag{4.15}$$

where in the gaussian noise term

$$N(\vec{k}_l) = 2A^2(\vec{k}_l)\int\frac{b^3\vec{k}_s}{(2\pi)^3}g^2(\vec{k}_s,\vec{k}_l-\vec{k}_s)P_{nl}(k_s)P_{nl}(|\vec{k}_l-\vec{k}_s|) \tag{4.16}$$

we neglected the shot noise which describes the fact that we can realize only an incomplete sampling of the density field [45]. The last equality in (4.15) is possible because, as we have said in Sec. 3.5, at large scales the non-linear power spectrum coincide with the linear one.

In order to minimize the noise, we choose for the weight g the form:

$$g(\vec{k}_s,\vec{k}_l-\vec{k}_s) = \frac{f(\vec{k}_s,\vec{k}_l-\vec{k}_s)}{2P_{nl}(k_s)P_{nl}(|\vec{k}_l-\vec{k}_s|)}. \tag{4.17}$$

In this way, we get:

$$N(\vec{k}_l) = A(\vec{k}_l) = \left[\int\frac{d^3\vec{k}_s}{(2\pi)^3}\frac{f^2(\vec{k}_s,\vec{k}_l-\vec{k}_s)}{2P_{nl}(k_s)P_{nl}(|\vec{k}_l-\vec{k}_s|)}\right]^{-1}. \tag{4.18}$$

Using the Fisher matrix formalism [49], we can define the error associated to measurements of the matter power spectrum for a set of narrow k-bins of width Δk: [3]

$$\delta P(k_l) = \frac{2\pi}{k_l\sqrt{V\Delta k}}\big(P_{nl}(k_l)+A(k_l)\big), \tag{4.19}$$

where V is the comoving volume used by a survey for measuring the matter power spectrum at k_l. The two terms on the r.h.s. of (4.19) account respectively for:

1. the *cosmic variance* due to the fact that we have access only to one Universe or, in terms of the ergodic hypothesis, to limited portions of the Universe [24];

2. the reconstruction noise due to the fact that we are doing an indirect estimation of the large scale structure.

Considering a toy survey of comoving volume $V = L^3$ and width $\Delta k = 2\pi/L = 2\pi/V^{1/3}$, we obtain:

$$\delta P(k_l) = \frac{(2\pi)^{1/2}}{k_l V^{1/3}}\big(P_{nl}(k_l)+A(k_l)\big). \tag{4.20}$$

[3] Actually, the definition is correct under the assumption that V is much larger than the scale of the features of the power spectrum so that $P(k)$ can be considered constant inside the Fourier cells $(2\pi)^3/V$ which, moreover, must be considered independent [45].

4.3 Light cone formalism

So far, we have neglected the redshift dependence focusing just on a snapshot. We observe a galaxy at distance x as it was at the time $z(x)$. Therefore, we do not have access to the full $\delta_m(\vec{k}, z)$ for every values of $\vec{k}$ inside the light cone[4], but just for the thin shell from which light, emitted at the time $z(x)$, has reached us [32]. To more efficiently reconstruct the large scales, we want to consider the spectrum defined inside the light cone, instead of individual snapshot at different z.

To do so, we need to define the matter power spectrum over the light-cone $P^{LC}(k)$, whose formulation is slightly more complicated than the one for the matter power spectrum at fixed redshift. In the works [32] and [57], an interesting description of the argument is provided.

In particular, following [57] we can introduce a useful approximated definition of $P^{LC}_{nl}(k)$ as the weighted average of the power spectrum over the survey comoving volume V, with weights given by the squared mean comoving number density $n(x)$ of objects at a given redshift:

$$\begin{aligned} P^{LC}_{nl}(k_l) &= \mathcal{N} \int dx \big[n(x)\, x\big]^2 P_{nl}(k,z) = \\ &= \mathcal{N} \int \frac{dz}{H(z)} \, \big[n(z)\, x(z)\big]^2 P_{nl}(k,z), \end{aligned} \tag{4.21}$$

with the normalization factor $\mathcal{N}$:

$$\mathcal{N} = \left\{ \int dx \big[n(x)\, x\big]^2 \right\}^{-1} = \left\{ \int \frac{dz}{H(z)} \, \big[n(z)\, x(z)\big]^2 \right\}^{-1}. \tag{4.22}$$

In both (4.21) and (4.22), in the last equality we rewrite the integral in term of redshift using the relation

$$dx = \frac{dz}{H(z)} \tag{4.23}$$

between z and the comoving coordinate x.

Finally, we introduce the bias factor we talked about in Sec. 3.6. Using the relation (3.21) for the bias, we obtain:

$$P^{LC}_{nl}(k_l) = \mathcal{N} \int \frac{dz}{H(z)} \big[n(z)\, b_0\, x(z)(1+z)\big]^2 P_{nl}(k,z), \tag{4.24}$$

with $\mathcal{N}$ the same as (4.22).

[4]The light cone is the locus of events in spacetime that can be causally connected to us [13].

It is useful to rewrite (4.24) and (4.22) as:

$$P_{nl}^{LC}(k_l) \simeq \mathcal{N} \sum_z \frac{\Delta z}{H(z)} \big[n(z)\ b_0\ x(z)(1+z)\big]^2 P_{nl}(k,z), \tag{4.25}$$

$$\mathcal{N} \simeq \left\{ \sum_z \frac{\Delta z}{H(z)}\ \big[n(z)\ x(z)\big]^2 \right\}^{-1}, \tag{4.26}$$

replacing the integral with a sum over the redshift bins Δz of the survey.

Once we have defined $P_{nl}^{LC}(k_l)$, we introduce the associated error. It can be proved [32] that the relations (4.18) and (4.19) are still valid substituting $P_{nl}(k_l)$ with $P_{nl}^{LC}(k_l)$.

Chapter 5

A case study: Euclid

In the last chapter we introduced the formalism of large scale structure reconstruction. In this chapter, we discuss an application of this formalism. The case study is the future survey *Euclid*.

Euclid is an ESA space telescope that will measure the shapes and the redshifts of galaxies over 15000 deg^2 on the sky and up to $z \sim 2$, thus allowing to explore the expansion history of the Universe. Its launch is planned for 2022 [1].

5.1 Euclid specifications

Being able to observe ~ 30 million galaxy redshifts, Euclid will measure galaxy clustering and reconstruct the matter power spectrum to percent accuracy [10] [54].

In this work we simulate Euclid performance. We assume observations at redshifts between $z = 0.90$ and $z = 1.80$, for a comoving volume $V = 19.7(\mathrm{h}^{-1}\mathrm{Gpc})^3$. We assume 4 redshift bins.

Bin width, central redshift and comoving number density of objects detected on average in each bin are taken from Ref. [10] and reported in Tab. 5.1.

Δz	z_m	$n(z)\left[(\mathrm{h\ Mpc}^{-1})^3\right]$
0.2	1	6.86×10^{-4}
0.2	1.2	5.58×10^{-4}
0.2	1.4	4.21×10^{-4}
0.3	1.65	2.61×10^{-4}

Table 5.1: Expected number density observed by Euclid. We assume that each redshift bin of width Δz is centered in z_m.

Parameter	Value
ω_b	0.022
ω_c	0.12
τ	0.07
A_s	2.1×10^{-9}
n_s	0.96
h	0.68
$\sum m_\nu$	0.06 eV
N_{eff}	3.046
b_0	0.73

Table 5.2: Reference Cosmological Parameters used for the standard dataset.

5.2 Large scale reconstruction

Using the aforementioned specifications and the relations (4.25) and (4.26), we construct a synthetic dataset consisting of 30 data points in the range of scale $0.02 \leq k\left[\text{h Mpc}^{-1}\right] \leq 0.20$. We refer to this dataset as *"standard"*. It will represent direct measurements of the matter power spectrum. The reference cosmological parameters used to realize the standard dataset via CAMB are in Table 5.2.

The error associated to the standard dataset is given by the cosmic variance[1]:

$$\delta P_{nl}^{LC}(k) = \frac{(2\pi)^{1/2}}{kV^{1/3}} P_{nl}^{LC}(k). \tag{5.1}$$

The standard dataset is shown in Fig. 5.1, together with the theoretical model. We then use the standard dataset to reconstruct the matter power spectrum at large scales, following the procedure outlined in Chapter 4.

Since we are observing a limited volume V, we can reconstruct the power spectrum for k_l modes that are spaced over $\Delta k = (2\pi)/V^{1/3}$. Therefore, the reconstruction allows to add to our dataset 9 data points whose errors are given by the relations (4.20) and (4.18). The integration in (4.18) has been performed in k_s over the range $k_{inf} \leq k_s \leq 0.20$ h Mpc^{-1}, with:

$$k_{inf} = \begin{cases} 0.02 \text{ h Mpc}^{-1}, & \textit{if } k_l \leq 0.005 \textit{ h Mpc}^{-1} \\ 2k_l, & \textit{otherwise} \end{cases} \tag{5.2}$$

to account for the squeezed limit $k_s \gg k_l$. The combination of the standard dataset with the additional data points represents our *"extended"* dataset. This is shown in Fig. 5.2: we can see that the reconstruction allowed to get information about the power spectrum until large scales of order $\mathcal{O}(10^{-4})$ that, otherwise, would have not been achieved.

[1] In our analysis we will neglect the shot noise: it is a good approximation for the scales and z we are considering.

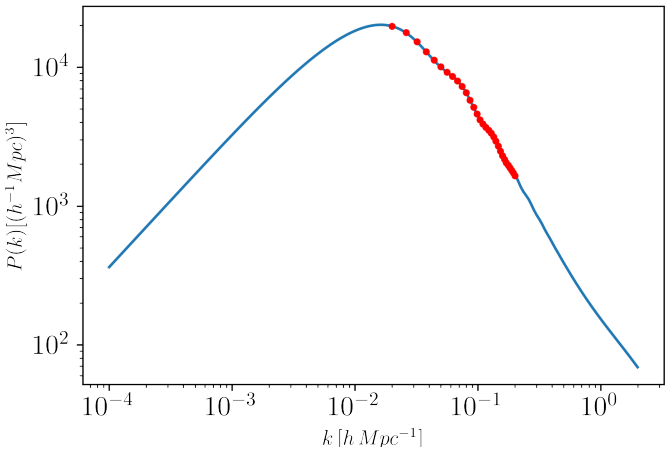

Figure 5.1: Light cone matter power spectrum with associated errors for the standard dataset.

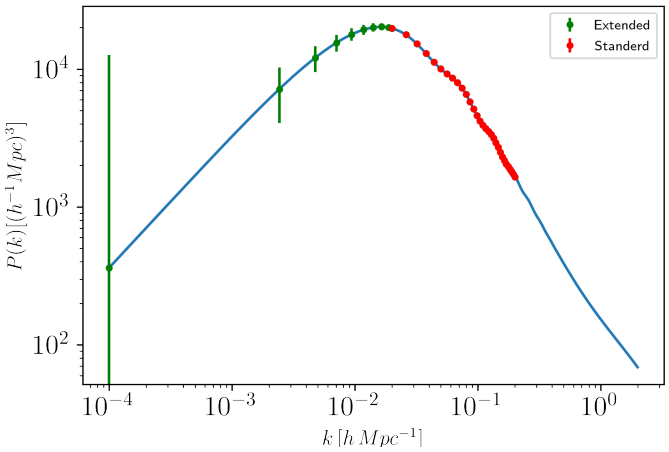

Figure 5.2: Light cone matter power spectrum with associated errors for the extended dataset: the green errorbars refers to the reconstructed data.

5.3 MCMC analysis

Once we reconstructed large scales matter power spectrum, we would like to investigate if and how introducing information about large scales improves our constraining power on cosmological parameters, in particular on $\sum m_\nu$.

To do so, we develop a code executing a Monte Carlo Markov Chains (MCMC) analysis on both datasets. We perform a statistical analysis in a bayesian framework. We write a likelihood module run on *Cobaya* (*co*de for *bay*esian *a*nalysis) software [15] [51] [52].
Cobaya is a framework for sampling and statistical modelling which allows to explore an arbitrary prior or posterior using an MC or MCMC sampler. It provides interfaces to cosmological theory codes as CAMB, too. Cobaya supports MPI parallelization. We exploit this feature to run our code on a HPC cluster provided by CINECA [4].

Our first step is the choice of the likelihood function, i.e. the probability of data given a model. In agreement with Ref. [49], a good choice is a Gaussian likelihood in $P^{LC}(k)$. To keep things simple, we assume a diagonal covariance with elements given by Eqs. (4.18), (4.20), (5.1).

The convergence for an MCMC run is achieved when $R - 1 \leq 0.01$.
R-1 is a generalized Gelman-Rubin statistics verifying that all chains are centered around the same point without deviations of significant fraction of the standard deviation of the posterior [22] [30]. The results of the sampling are analysed with *GetDist* [3] [31]. We show the results in the figures in this way:

- black lines refer to the standard dataset, while red lines to the extended;
- thin dashed blue lines show the reference values;
- the concentric lines in the triangle plot describe the probability contours of 68% (internal line) and 95% (external line) confidence level (CL).

In the code, we vary one or more parameters from Tab. 5.2. We assume either uniform or normal prior distribution in order to observe different behaviours depending on the dataset we analysed.

Firstly, we take some exploratory tests, to check that our analysis is unbiased, i.e., that we are able to recover the fiducial values. We verify it varying $\sum m_\nu$. As we can see from Fig. 5.3, our analysis is unbiased, since we recover $\sum m_\nu = 0.06$ eV with both datasets.

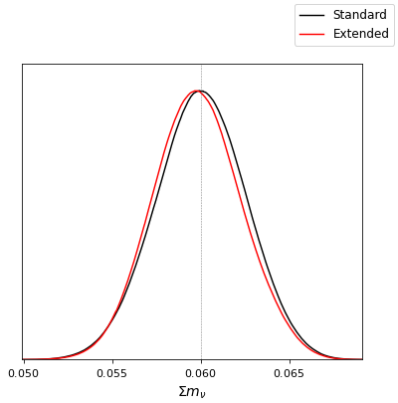

Figure 5.3: Posterior probability distribution of $\sum m_\nu$ when varying only $\sum m_\nu$ with a uniform prior.

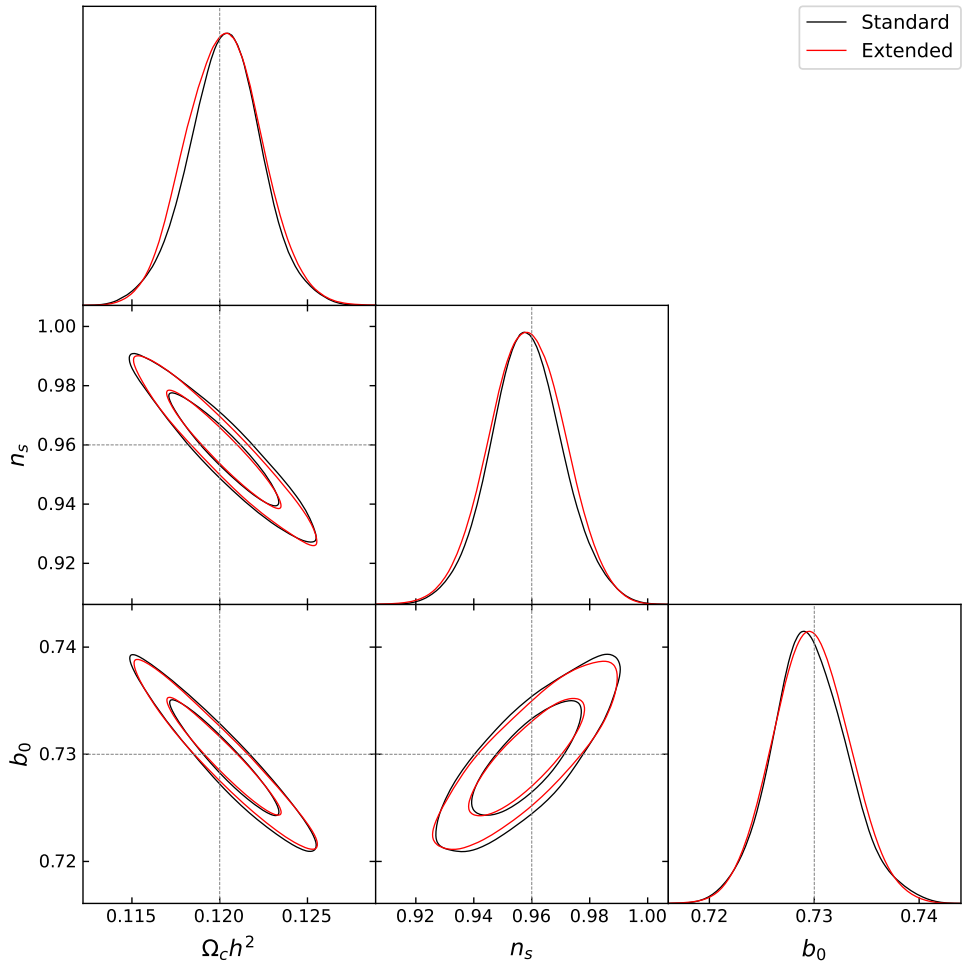

Figure 5.4: Posterior probability distributions when varying ω_c,n_s and b_0 with uniform priors.

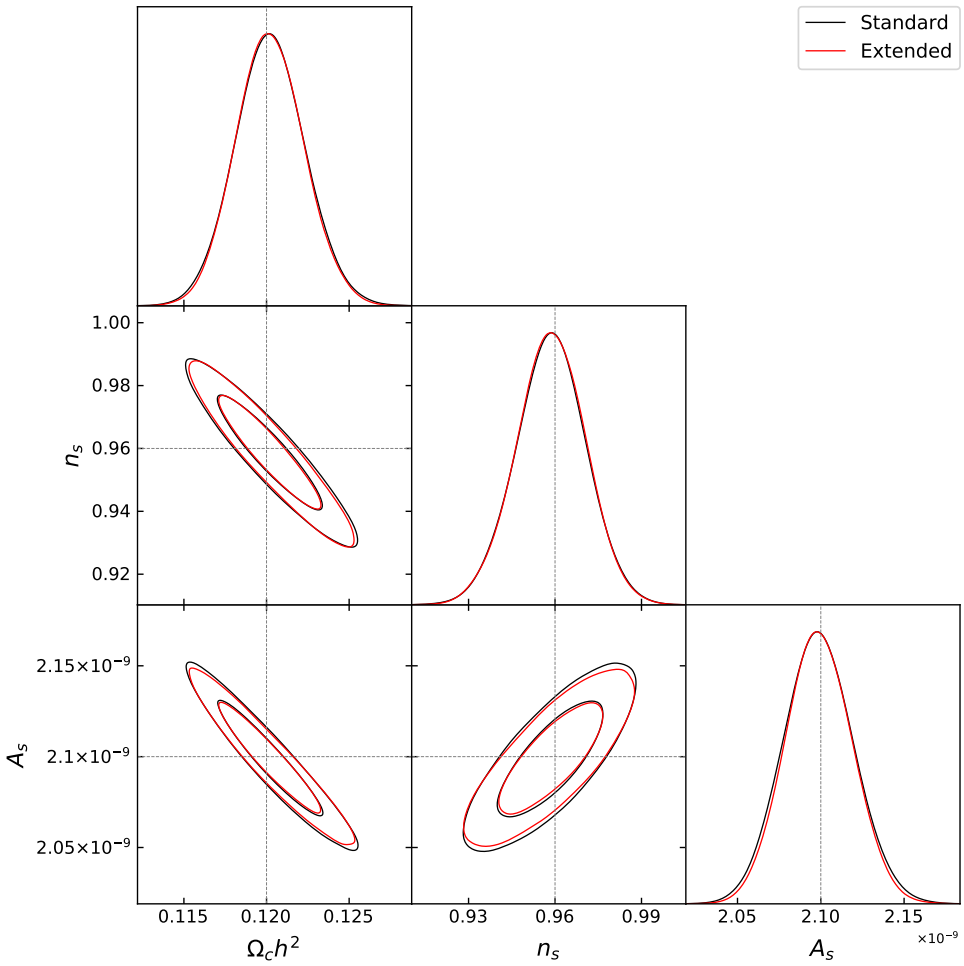

Figure 5.5: Posterior probability distributions when varying ω_c,n_s and A_s with uniform priors.

As we have already said in the Sec. 3.4, varying two o more parameters allows to counteract background effects from $\sum m_\nu$ lightening up the perturbations ones. We expect some degeneracies between them: it is interesting analysing if adding informations from large scales helps breaking these degeneracies in order to separate the effects of parameters on the matter power spectrum.

Firstly, we investigate what happens keeping $\sum m_\nu = 0.06$ eV constant. We start varying ω_c [2], n_s and b_0 using a uniform prior (Fig. 5.4).

Later we substitute b_0 with A_s using a uniform prior (Fig. 5.5). Both in Fig. 5.4 and 5.5 we can observe a regular behaviour in the posterior distributions with little constraining improvements using the extended dataset.

[2] In all the figures, there is the label $\Omega_c h^2$ instead of ω_c.

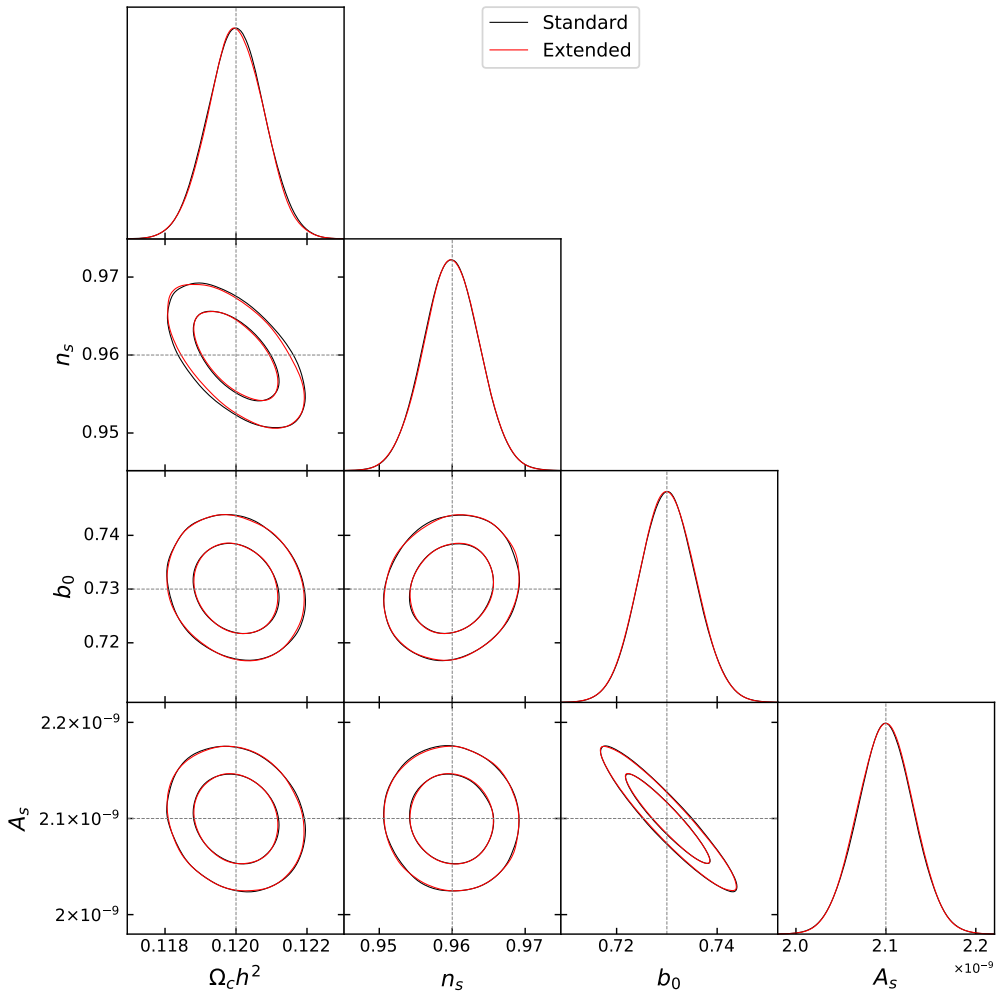

Figure 5.6: Posterior probability distributions when varying ω_c,n_s,A_s and b_0 with normal priors.

Keeping $\sum m_\nu$ fixed, we vary ω_c,n_s,A_s and b_0 with normal priors (Fig. 5.6). In particular, the width of the prior for b_0 is chosen following Ref. [46]. In this case, we have just two degeneracies $\omega_c - n_s$ and $A_s - b_0$ which share the same degeneracy direction: when the first parameter increases, the second one decreases. This happens because, as we can see in Figs. 5.7, 5.8 and Figs. 5.9, 5.10 each parameter pair shows the same effect on the matter power spectrum.

In this case, the differences between the standard and the extended datasets are negligible.

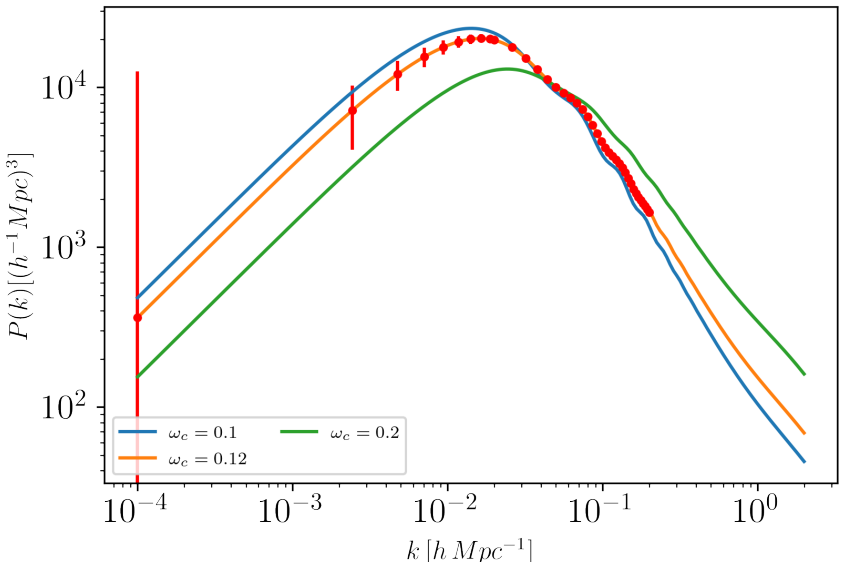

Figure 5.7: Extended dataset with theoretical models for increasing ω_c.

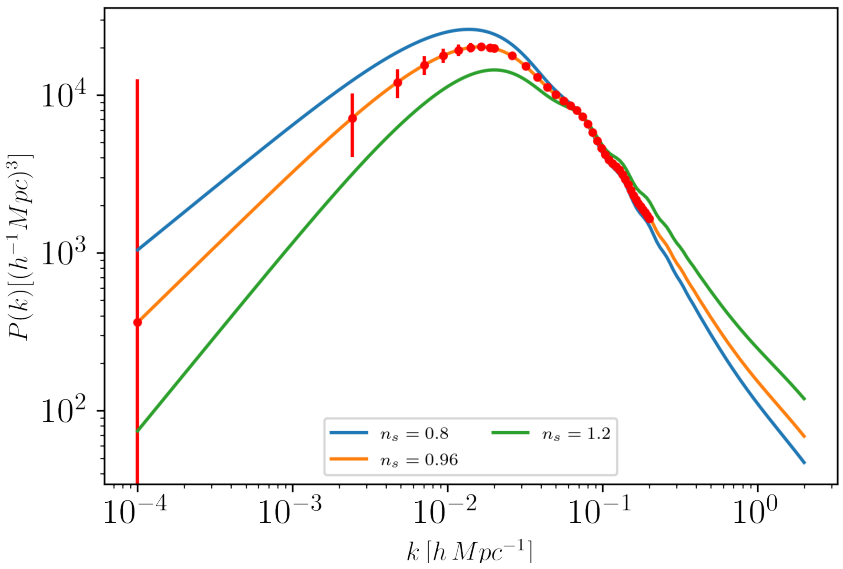

Figure 5.8: Extended dataset with theoretical models for increasing n_s.

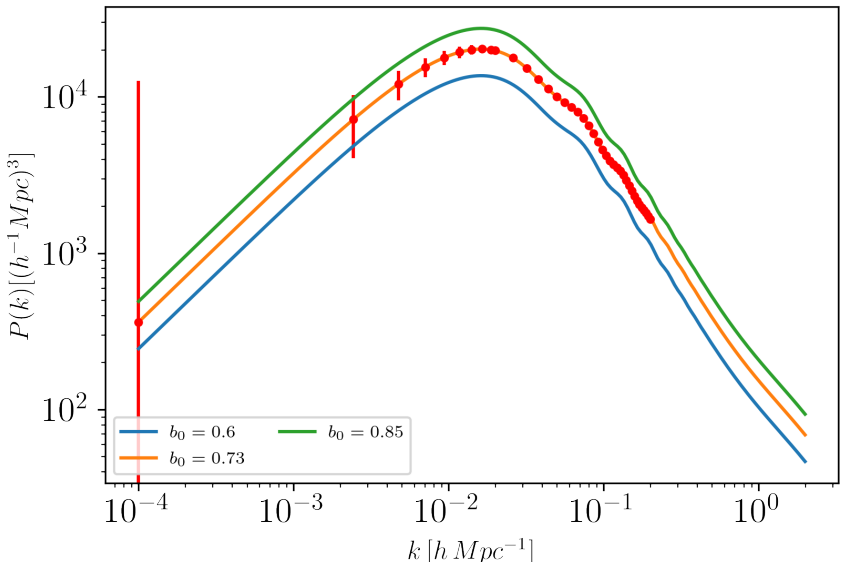

Figure 5.9: Extended dataset with theoretical models for increasing b_0.

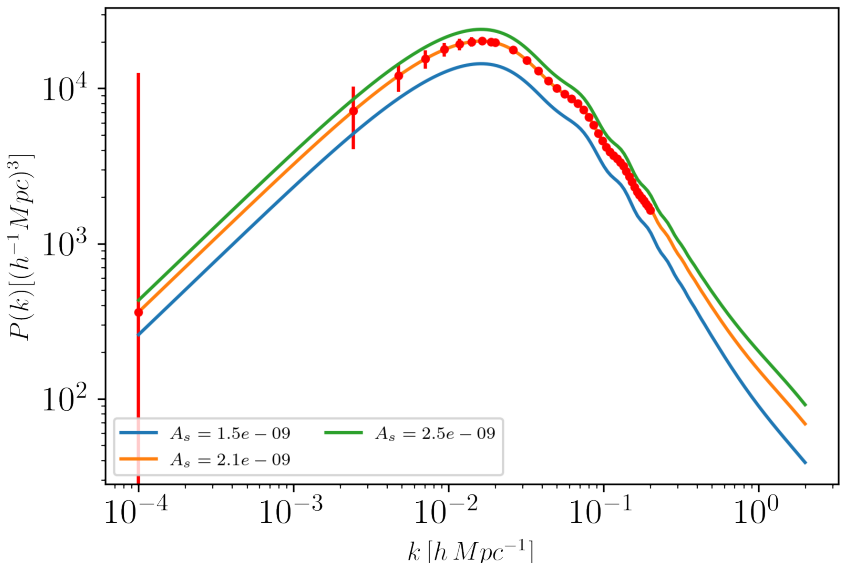

Figure 5.10: Extended dataset with theoretical models for increasing A_s.

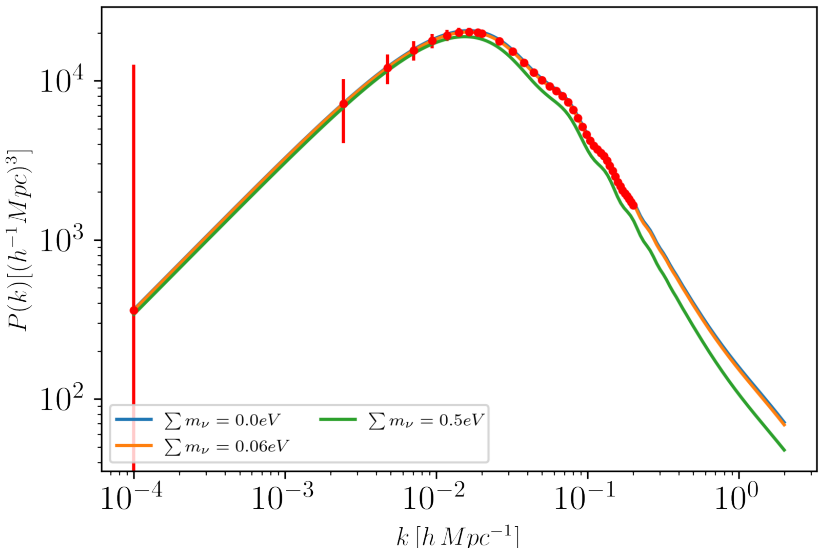

Figure 5.11: Extended dataset with theoretical models for increasing m_ν.

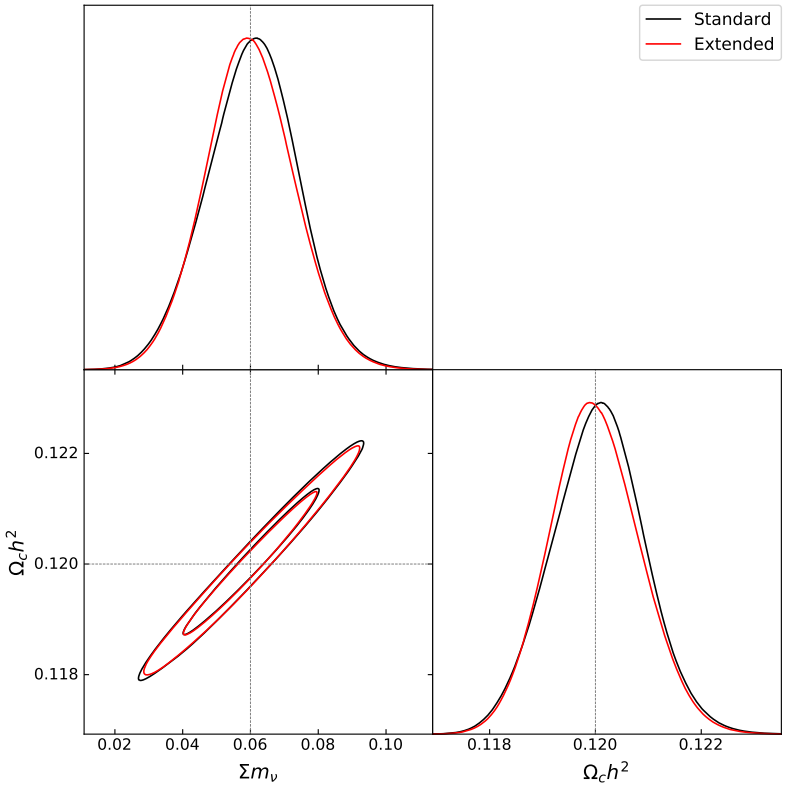

Figure 5.12: Posterior probability distributions when varying $\sum m_\nu$ and ω_c with uniform priors.

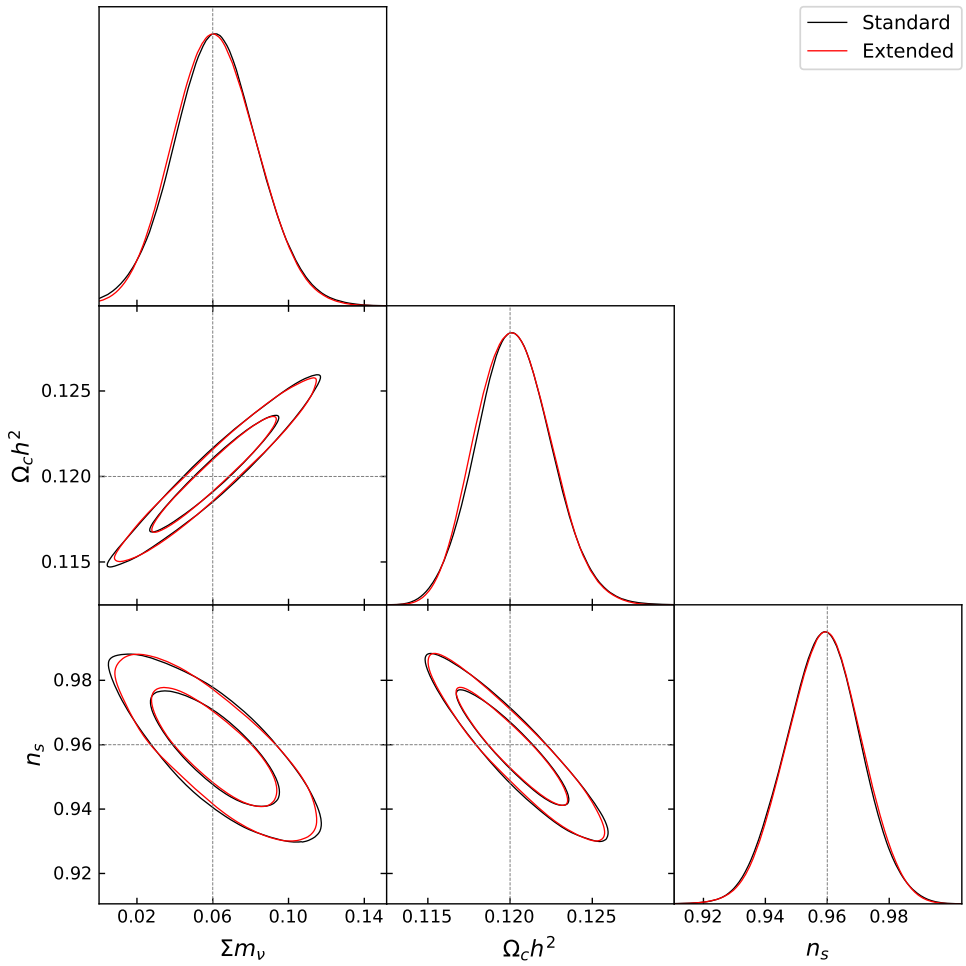

Figure 5.13: Posterior probability distributions when varying m_ν, ω_c and n_s with uniform priors.

Now, let us introduce $\sum m_\nu$ as a variable parameter adding gradually other parameters.

From both the triangle plots in Fig. 5.12 and 5.13 we can see the degeneracy between ω_c and $\sum m_\nu$. As we can understand looking at Fig. 5.11 and 5.7, $\sum m_\nu$ suppresses at small scales the matter power spectrum. The latter increases with ω_c at the same scales. Therefore, if $\sum m_\nu$ increases, ω_c has to decrease in order to keep the matter power spectrum constant.

On the contrary, as we can see by comparing Fig. 5.11 and 5.8, the degeneracy $\sum m_\nu - n_s$ in Fig. 5.13 happens because the matter power spectrum is almost constant at large scale with respect to $\sum m_\nu$, while at the same scales the matter power spectrum strongly decreases with n_s.

Looking at Fig. 5.12 and 5.13, we notice a mild improvement of the 2D contours when adding the extended dataset. This is due to the fact that

the extended dataset helps to constrain the impact of the parameter both at large and small scales.

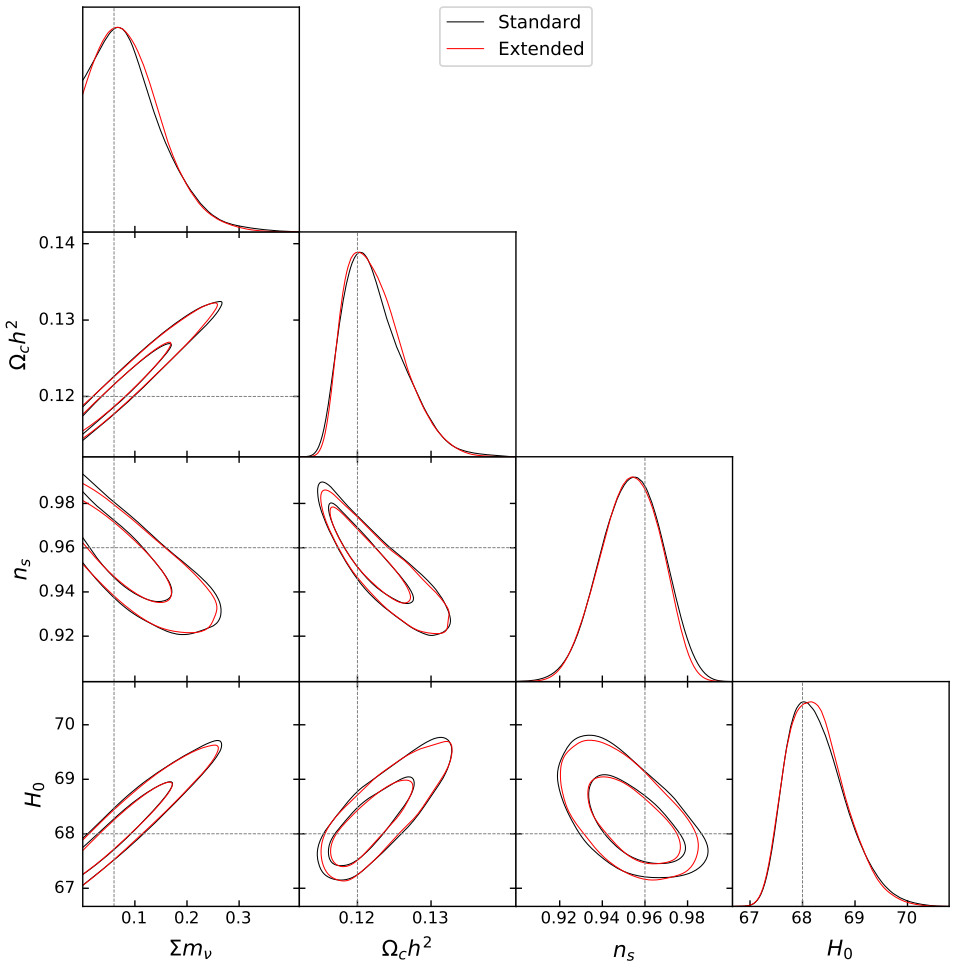

Figure 5.14: Posterior probability distributions when varying $\sum m_\nu$, ω_c, n_s and H_0 with uniform priors.

We then vary H_0 with a uniform prior. The triangle plot 5.14 shows the same degeneracies as in Fig. 5.13, even though with slightly deformed shapes due to the fact we add the new variable parameter H_0. We can see a degeneracy $\sum m_\nu - H_0$. As we can see in Fig. 5.15, the matter power spectrum increases with H_0. Therefore, to compensate the suppression induced by $\sum m_\nu$, H_0 increases with $\sum m_\nu$.

It is relevant to underline that, using the extended dataset, we can appreciate a little improvement in the constraining power on ω_c, n_s and H_0. This is reasonable because, as we can see looking at Figs. 5.7, 5.8 and 5.15, they all affect the large scales.

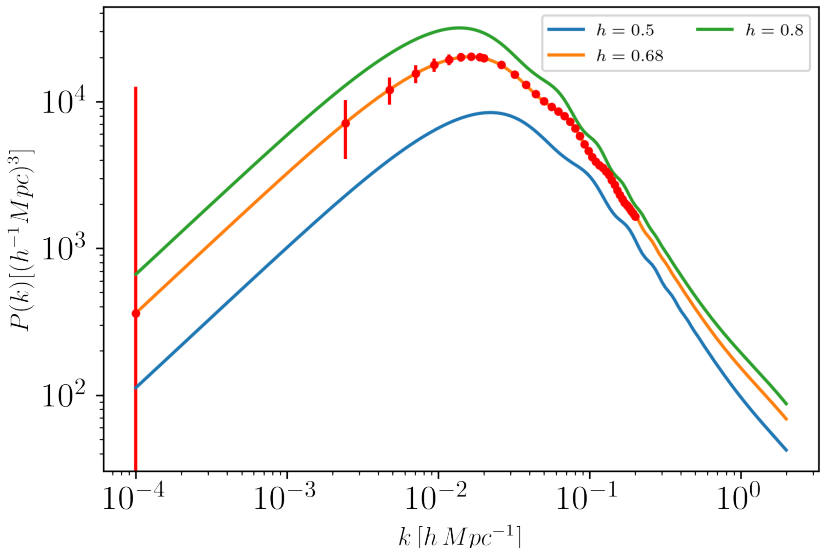

Figure 5.15: Extended dataset with theoretical models for increasing h. Throughout this section we will use the dimensional Hubble-Lemaître constant H_0 instead of the dimensionless h.

Varying the bias b_0 instead of H_0 using a uniform prior produces the interesting triangle plot in Fig. 5.16. In this case we only have an upper bound on $\sum m_\nu$ and a very wide posterior on b_0. This is due to the very strong degeneracy between $\sum m_\nu$ and b_0. The degeneracy $\sum m_\nu - \omega_c$ is broken. The inversion of the degeneracy direction between $\sum m_\nu$ and n_s with respect to the triangle plot 5.13 is another interesting effects.

These behaviours are likely caused by the strong degeneracies $b_0 - \sum m_\nu$ and $b_0 - n_s$. We have seen above that increasing $\sum m_\nu$ suppresses the power spectrum; on the other hand, according to (3.20), the matter power spectrum increases with b_0 (see Fig. 5.9).

At the same time, at large scales the power spectrum strongly decreases with n_s. As a consequence, b_0 increases with n_s. These degeneracies cause the inversion of the degeneracy direction between $\sum m_\nu$ and n_s. The effects we have described are also strong enough to destroy the degeneracies of ω_c with $\sum m_\nu$ and n_s.

To summarize: adding the new parameter b_0 changes the relations between the other parameters. This shows how important the research on bias is. Its limited knowledge is one of the principal limits to improved sensitivity and a major topic of theoretical studies [17].

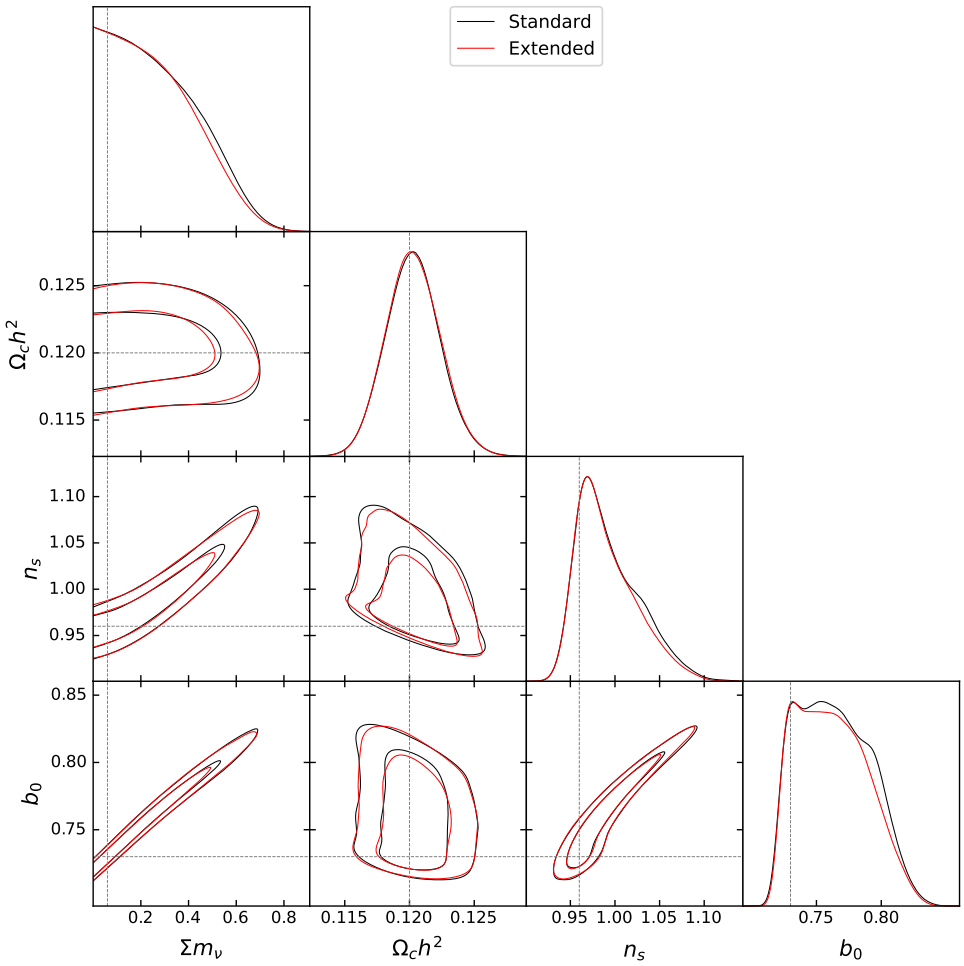

Figure 5.16: Posterior probability distributions when varying $\sum m_\nu$, ω_c, n_s and b_0 with uniform priors.

In Fig. 5.17 we vary b_0 with a normal prior. In this way, the MCMC run is able to recover the reference value of $\sum m_\nu$, in particular for the extended dataset. Furthermore, the b_0 posterior distribution improves with respect to the previous case. Since the gaussian prior prevents b_0 from varying over a wide range, we also notice that a small correlation between ω_c and $\sum m_\nu$ appears, contrary to the previous case.

In both the Fig. 5.16 and 5.17 we see that the extended dataset provides a better constraining power on n_s, ω_c(as said before) and also b_0, due to the fact that b_0 is sensitive to the large scales (see Fig. 5.9).

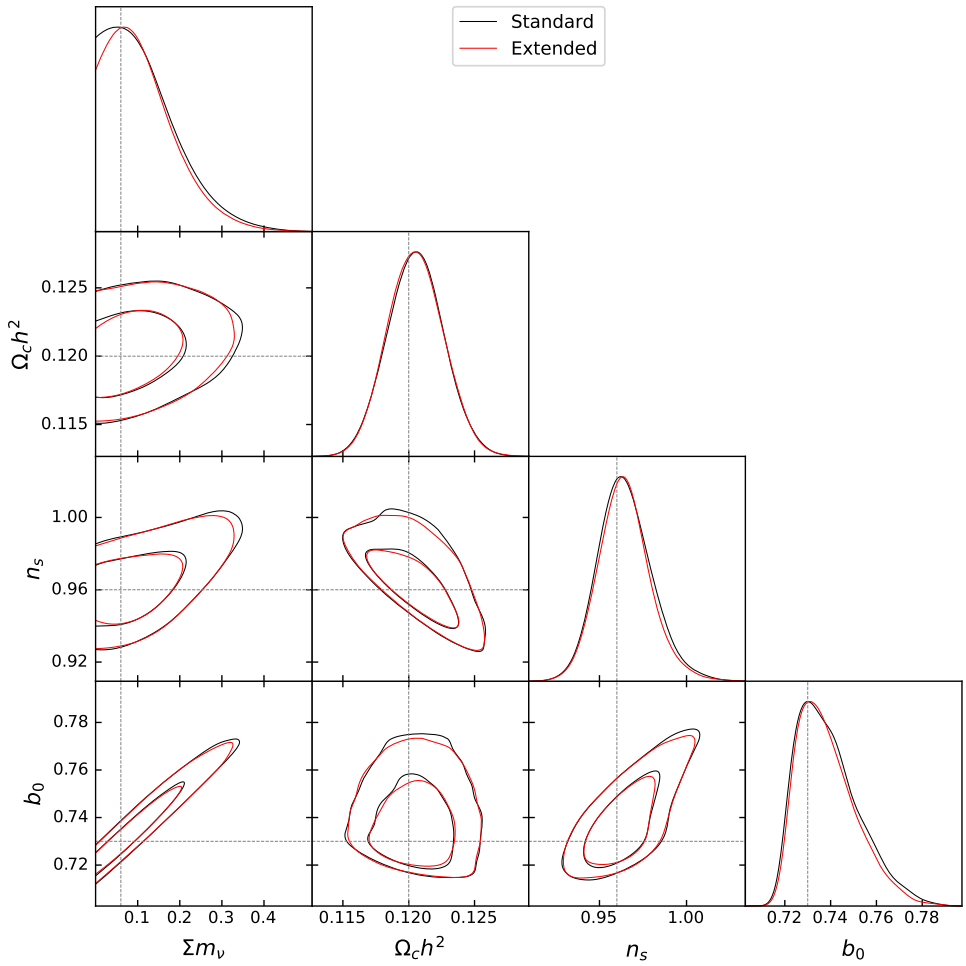

Figure 5.17: Posterior probability distributions when varying $\sum m_\nu$, ω_c, n_s with uniform priors and b_0 with normal prior.

It is interesting to analyse how the previous Fig. 5.14 and 5.16 change in case of a normal prior for all the parameters. The width of the prior distribution is chosen to resemble the constraining power from CMB data (e.g., Planck [6]).

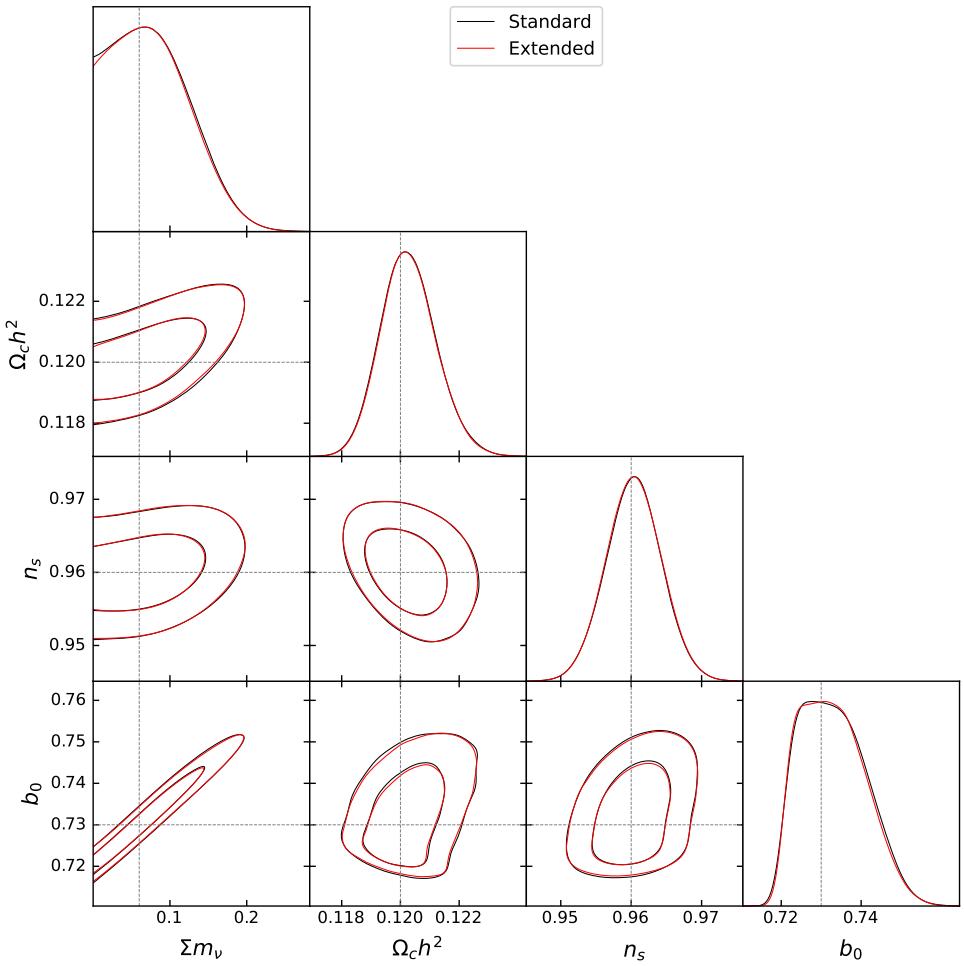

Figure 5.18: Posterior probability distributions when varying $\sum m_\nu$, ω_c, n_s and b_0 with normal priors.

If we vary b_0, $\sum m_\nu$, ω_c and n_s we obtain the triangle plot 5.18 which is similar to Fig. 5.17 apart from the fact that the improvements obtained using the extended dataset are almost negligible, for this set of parameters.

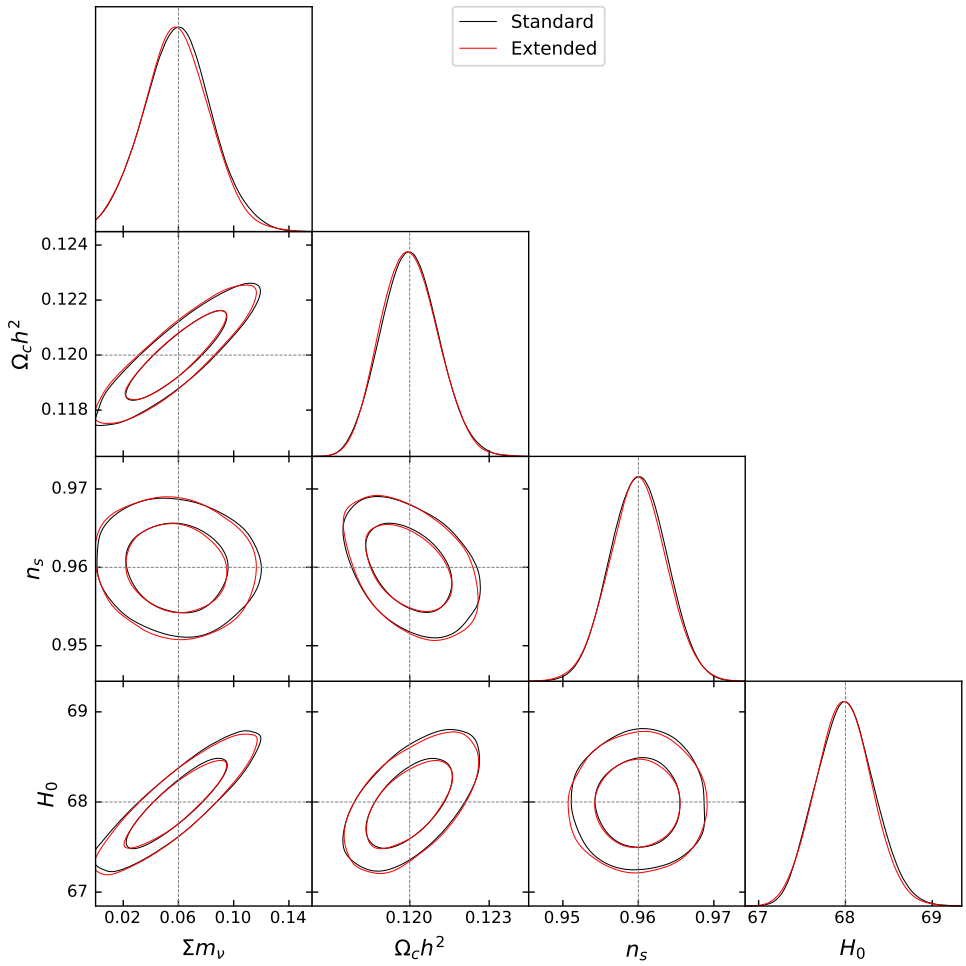

Figure 5.19: Posterior probability distributions when varying $\sum m_\nu$, ω_c, n_s and b_0 with normal priors.

If we vary H_0, $\sum m_\nu$, ω_c and n_s, with respect to Fig. 5.14, in the triangle plot 5.19:

- we recover the reference value for the n_s posterior distribution;
- we break the $\sum m_\nu - n_s$ and $H_0 - n_s$ degeneracies;
- the improvements obtained using the extended dataset are mild.

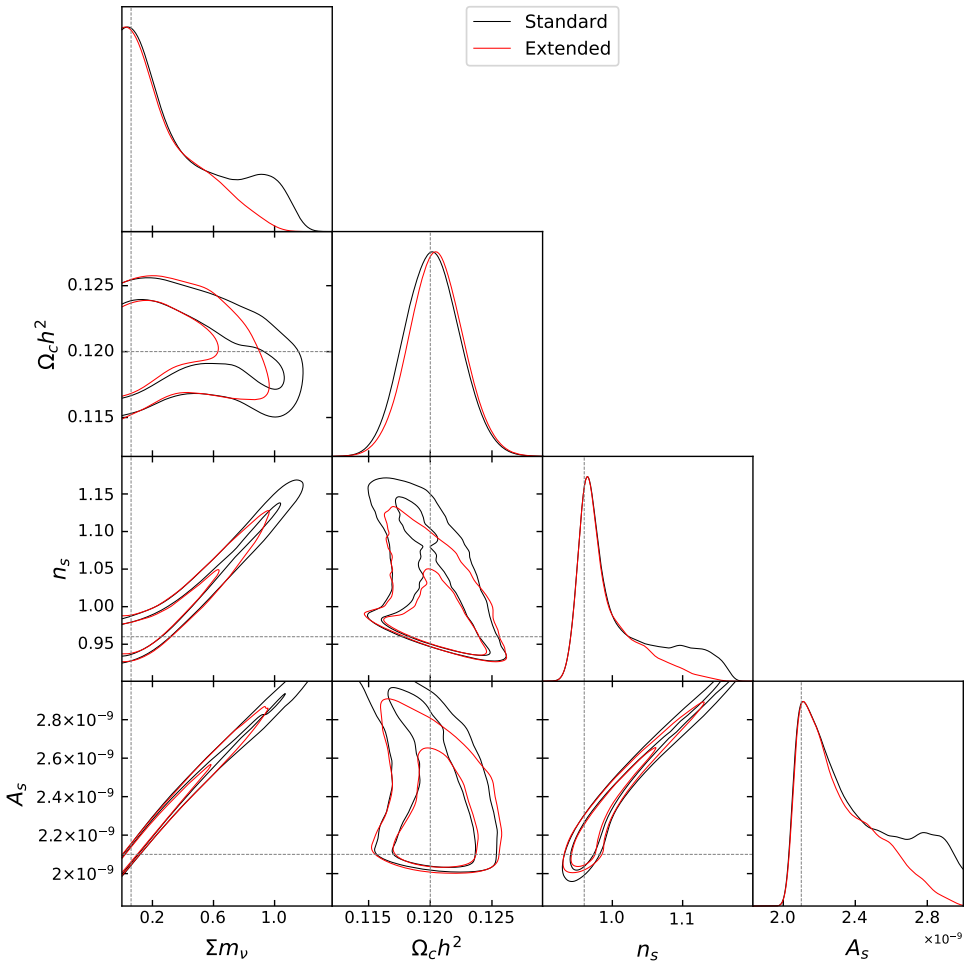

Figure 5.20: Posterior probability distributions when varying $\sum m_\nu$, ω_c,n_s and A_s with uniform priors.

We now focus on what happens when we vary also the A_s parameter. We start varying $\sum m_\nu$, ω_c,n_s and A_s with uniform priors (Fig. 5.20).

First of all, it is important to focus on the degeneracies. Immediately we can see a really strong $A_s - \sum m_\nu$ degeneracy: even in this case it is a compensation effect between the neutrino suppression and the increase of the matter power spectrum with A_s (see Fig. 5.10). Similarly, we can explain the $n_s - A_s$ degeneracy as a compensation effect at large scales.

These degeneracies are so strong to invert the direction of degeneracy $\sum m_\nu - n_s$ and destroying the degeneracies $\omega_c - \sum m_\nu$ and $n_s - \omega_c$ we have seen in 5.13 and 5.14.

Let us underline that we have already seen analogue characteristics in the triangle plot 5.16 of b_0: both of them show similar 2D contours.
This is in agreement with the degeneracy between A_s and b_0 we observed

in Fig. 5.6.

In the triangle plot 5.20 we can also appreciate a big improvement in the constraining power for almost all the distributions when we use the extended dataset: the inclusion of the large scales helps to better constrain A_s and, in turn, the other degenerate parameters.

Comparing the Fig. 5.16 and 5.20 with the triangle plots and 5.4 5.5 highlights that assuming $\sum m_\nu$ variable causes some distortions in the posterior distributions and removes also the degeneracies $b_0 - \omega_c$, $A_s - \omega_c$ and $n_s - \omega_c$. Furthermore, it is evident that adding information from large scale, i.e. using the extended dataset, is helpful in constraining the cosmological parameters when we assume $\sum m_\nu$ not fixed.

To conclude, we have shown that the use of the extended dataset can, in some cases, improve the constraints on cosmological parameters. Depending on the set of varying parameters and on their prior knowledge, the improvement can be mild. Nevertheless, we have demonstrated that the inclusion of information about large scale is particularly useful to constrain those parameters that are mostly degenerate with $\sum m_\nu$ and affect the shape of the matter power spectrum at all scales, i.e. , A_s and b_0.
Larger improvements are expected if more extended cosmological models are considered, and/or a more complex expression for the bias is used (for example, a scale-dependent bias). The work presented in this thesis sets the basis for future studies in this direction.

Conclusions

In this thesis we have realized a complete pipeline to study the impact of the addition of information about large scale modes of the matter power spectrum on cosmological constraints. We have reviewed the theoretical background about cosmological perturbations and developed the formalism of large scale structure reconstruction. We proceeded in this way:

1. study of the formalism of large-scale reconstruction;
2. development of a computational tool for the reconstruction of large scales from the small scale observable matter power spectrum;
3. simulation of performances on synthetic data from a future survey;
4. application to a cosmological model;
5. realization of a code for an MCMC bayesian analysis run on a HPC cluster;
6. analysis and study of the MCMC results.

We applied this pipeline to the simple case of the ΛCDM+$\sum m_\nu$ model using the Euclid survey as a toy model. We have seen that, for this model, including information about large scale is particularly useful to constrain those parameters that are mostly degenerate with $\sum m_\nu$ and affect the shape of the matter power spectrum at all scales, i.e. , the amplitude of the primordial matter power spectrum A_s and the galaxy bias b_0.

Despite being very simple, the present work sets the basis for immediate extensions. For example:

- addition of redshift space distortions effects, combination with other cosmological datasets (e.g. CMB [10]), study of extended cosmological models (e.g. with dynamical dark energy [58] or curvature $\Omega_k \neq 0$ [55]) and more complex expressions for the bias [17];
- calculation of more realistic data covariance and more refined likelihood function;

- application to N-body simulations for testing the reconstruction on more realistic synthetic datasets [33] [32].

Finally, it could be interesting also to go to higher order in perturbation theory for the matter perturbations to achieve higher order corrections of our results.

To conclude, through our simple and self-contained pipeline, we have shown that is worth exploring the potential of the large-scale reconstruction method to study cosmologies beyond the standard ΛCDM.

Bibliography

[1] URL: https://sci.esa.int/web/euclid.

[2] URL: https://camb.info/.

[3] URL: https://getdist.readthedocs.io/en/latest/index.html.

[4] URL: https://www.hpc.cineca.it/.

[5] P. A. R. Ade et al. "Planck 2013 results. XXII. Constraints on inflation". In: *Astron. Astrophys.* 571 (2014), A22. DOI: 10.1051/0004-6361/201321569. arXiv: 1303.5082 [astro-ph.CO].

[6] N. Aghanim et al. "Planck 2018 results". In: 641 (Sept. 2020), A6. ISSN: 1432-0746.

[7] Francisco Villaescusa-Navarro et al. "Cosmology with massive neutrinos I: towards a realistic modeling of the relation between matter, haloes and galaxies". In: *JCAP03(2014)011* (2013).

[8] Jack J. Bennett et al. *Towards a precision calculation of $N_{\rm eff}$ in the Standard Model II: Neutrino decoupling in the presence of flavour oscillations and finite-temperature QED*. 2021. arXiv: 2012.02726 [hep-ph].

[9] F. Bernardeau et al. "Large-scale structure of the Universe and cosmological perturbation theory". In: *Physics Reports* 367.1-3 (Sept. 2002), pp. 1–248. ISSN: 0370-1573. DOI: 10.1016/s0370-1573(02)00135-7. URL: http://dx.doi.org/10.1016/S0370-1573(02)00135-7.

[10] A. Blanchard et al. "Euclid preparation. VII. Forecast validation for Euclid cosmological probes". In: *Astronomy and Astrophysics* 642 (Oct. 2020).

[11] Michael R. Blanton et al. "Sloan Digital Sky Survey IV: Mapping the Milky Way, Nearby Galaxies, and the Distant Universe". In: *aj* 154.1, 28 (July 2017), p. 28. DOI: 10.3847/1538-3881/aa7567. arXiv: 1703.00052 [astro-ph.GA].

[12] F. Capozzi et al. "Neutrino masses and mixings: Status of known and unknown 3 ν parameters". In: *Nuclear Physics B* 908 (July 2016), pp. 218–234. ISSN: 0550-3213. DOI: 10.1016/j.nuclphysb.2016.02.016. URL: http://dx.doi.org/10.1016/j.nuclphysb.2016.02.016.

[13] Sean Carroll. *Spacetime and Geometry: An Introduction to General Relativity*. Benjamin Cummings, 2003. ISBN: 0805387323. URL: http://www.amazon.com/Spacetime-Geometry-Introduction-General-Relativity/dp/0805387323.

[14] Emanuele Castorina et al. "Cosmology with massive neutrinos II: on the universality of the halo mass function and bias". In: *JCAP* 02 (2014), p. 049. DOI: 10.1088/1475-7516/2014/02/049. arXiv: 1311.1212 [astro-ph.CO].

[15] *Cobaya documentation*. URL: https://cobaya.readthedocs.io/en/latest/index.html#.

[16] P.F. de Salas et al. "Status of neutrino oscillations 2018: 3σ hint for normal mass ordering and improved CP sensitivity". In: *Physics Letters B* 782 (2018), pp. 633–640.

[17] Vincent Desjacques, Donghui Jeong, and Fabian Schmidt. "Large-scale galaxy bias". In: *Physics Reports* 733 (Feb. 2018), pp. 1–193. ISSN: 0370-1573. DOI: 10.1016/j.physrep.2017.12.002. URL: http://dx.doi.org/10.1016/j.physrep.2017.12.002.

[18] Nathaniel Dick. "Quantifying the Inhomogeneous Distribution of Matter by Perturbing the Smooth Universe". 2018.

[19] Nathaniel Dick. "Quantifying the Inhomogeneous Distribution of Matter by Perturbing the Smooth Universe". PhD thesis. 2018.

[20] A.D. Dolgov. "Neutrinos in cosmology". In: *Physics Reports* 370.4-5 (Nov. 2002), pp. 333–535. ISSN: 0370-1573. DOI: 10.1016/s0370-1573(02)00139-4. URL: http://dx.doi.org/10.1016/S0370-1573(02)00139-4.

[21] Jaan Einasto. *Dark Matter*. 2010. arXiv: 0901.0632 [astro-ph.CO].

[22] Andrew Gelman and Donald B. Rubin. "Inference from Iterative Simulation Using Multiple Sequences". In: *Statistical Science* 7.4 (1992), pp. 457–472. DOI: 10.1214/ss/1177011136. URL: https://doi.org/10.1214/ss/1177011136.

[23] Martina Gerbino et al. "Likelihood Methods for CMB Experiments". In: *Frontiers in Physics* 8 (2020), p. 15. ISSN: 2296-424X. DOI: 10.3389/fphy.2020.00015. URL: https://www.frontiersin.org/article/10.3389/fphy.2020.00015.

[24] Marc Kamionkowski and Abraham Loeb. "Getting around cosmic variance". In: *Phys. Rev. D* 56 (1997), pp. 4511–4513. DOI: 10.1103/PhysRevD.56.4511. arXiv: astro-ph/9703118.

[25] David Langlois. “Inflation, Quantum Fluctuations and Cosmological Perturbations”. In: *Particle Physics and Cosmology: The Interface*. Ed. by D. Kazakov and G. Smadja. Dordrecht: Springer Netherlands, 2005, pp. 235–278. ISBN: 978-1-4020-3161-8.

[26] Massimiliano Lattanzi and Martina Gerbino. *Status of neutrino properties and future prospects - Cosmological and astrophysical constraints*. 2017. arXiv: 1712.07109 [astro-ph.CO].

[27] J LESGOURGUES and S PASTOR. “Massive neutrinos and cosmology”. In: *Physics Reports* 429.6 (July 2006), pp. 307–379. ISSN: 0370-1573. DOI: 10.1016/j.physrep.2006.04.001. URL: http://dx.doi.org/10.1016/j.physrep.2006.04.001.

[28] Julien Lesgourgues et al. “Neutrino Cosmology”. In: Cambridge University Press, 2013, pp. 273–347. DOI: 10.1017/CBO9781139012874.

[29] Julien Lesgourgues et al. *Neutrino Cosmology*. Cambridge University Press, 2013. DOI: 10.1017/CBO9781139012874.

[30] Antony Lewis. “Efficient sampling of fast and slow cosmological parameters”. In: *Physical Review D* 87.10 (May 2013). ISSN: 1550-2368. DOI: 10.1103/physrevd.87.103529. URL: http://dx.doi.org/10.1103/PhysRevD.87.103529.

[31] Antony Lewis. “GetDist: a Python package for analysing Monte Carlo samples”. In: (2019). arXiv: 1910.13970 [astro-ph.IM]. URL: https://getdist.readthedocs.io.

[32] Peikai Li, Rupert A. C. Croft, and Scott Dodelson. *Large Scale Structure Reconstruction with Short-Wavelength Modes: Halo Bias and Light Cone Formalism*. 2020. arXiv: 2007.00226 [astro-ph.CO].

[33] Peikai Li, Scott Dodelson, and Rupert A. C. Croft. “Large scale structure reconstruction with short-wavelength modes”. In: *Physical Review D* 101.8 (Apr. 2020). ISSN: 2470-0029. DOI: 10.1103/physrevd.101.083510. URL: http://dx.doi.org/10.1103/PhysRevD.101.083510.

[34] Jia Liu et al. “MassiveNuS: cosmological massive neutrino simulations”. In: *Journal of Cosmology and Astroparticle Physics* 2018.03 (Mar. 2018), pp. 049–049. ISSN: 1475-7516. DOI: 10.1088/1475-7516/2018/03/049. URL: http://dx.doi.org/10.1088/1475-7516/2018/03/049.

[35] Marilena LoVerde. “Halo bias in mixed dark matter cosmologies”. In: *Phys. Rev. D* 90 (8 Oct. 2014), p. 083530. DOI: 10.1103/PhysRevD.90.083530. URL: https://link.aps.org/doi/10.1103/PhysRevD.90.083530.

[36] Marilena LoVerde. "Spherical collapse in $\nu\Lambda$ CDM". In: *Phys. Rev. D* 90.8 (2014), p. 083518. DOI: 10.1103/PhysRevD.90.083518. arXiv: 1405.4858 [astro-ph.CO].

[37] Gianpiero Mangano et al. "Relic neutrino decoupling including flavour oscillations". In: *Nuclear Physics B* 729.1-2 (Nov. 2005), pp. 221–234. ISSN: 0550-3213. DOI: 10.1016/j.nuclphysb.2005.09.041. URL: http://dx.doi.org/10.1016/j.nuclphysb.2005.09.041.

[38] Chirag Modi et al. "Reconstructing large-scale structure with neutral hydrogen surveys". In: *Journal of Cosmology and Astroparticle Physics* 2019.11 (Nov. 2019), pp. 023–023. ISSN: 1475-7516. DOI: 10.1088/1475-7516/2019/11/023. URL: http://dx.doi.org/10.1088/1475-7516/2019/11/023.

[39] P.J.E. Peebles. "Statistical Analysis of Catalogs of Extragalactic Objects. I. Theory". In: *apj* 185 (Oct. 1973), pp. 413–440. DOI: 10.1086/152431.

[40] *PLANCK experiment*. URL: https://www.cosmos.esa.int/web/planck.

[41] Brian Albert Robson. "Introductory Chapter: Standard Model of Cosmology". In: *Redefining Standard Model Cosmology*. Ed. by Brian Albert Robson. Rijeka: IntechOpen, 2019. Chap. 1. DOI: 10.5772/intechopen.85605. URL: https://doi.org/10.5772/intechopen.85605.

[42] Pablo F. de Salas and Sergio Pastor. "Relic neutrino decoupling with flavour oscillations revisited". In: *JCAP* 07 (2016), p. 051. DOI: 10.1088/1475-7516/2016/07/051. arXiv: 1606.06986 [hep-ph].

[43] Subir Sarkar. "Measuring the baryon content of the universe: BBN vs CMB". In: (June 2002).

[44] Douglas Scott. *The Standard Model of Cosmology: A Skeptic's Guide*. 2018. arXiv: 1804.01318 [astro-ph.CO].

[45] Hee-Jong Seo and Daniel J. Eisenstein. "Probing Dark Energy with Baryonic Acoustic Oscillations from Future Large Galaxy Redshift Surveys". In: *The Astrophysical Journal* 598.2 (Dec. 2003), pp. 720–740. ISSN: 1538-4357. DOI: 10.1086/379122. URL: http://dx.doi.org/10.1086/379122.

[46] Tim Sprenger et al. "Cosmology in the era of Euclid and the Square Kilometre Array". In: *Journal of Cosmology and Astroparticle Physics* 2019 (Jan. 2018). DOI: 10.1088/1475-7516/2019/02/047.

[47] Markus Steidl. *KATRIN*. URL: https://www.katrin.kit.edu/.

[48] R. Takahashi. "Third-Order Density Perturbation and One-Loop Power Spectrum in Dark-Energy-Dominated Universe". In: *Progress of Theoretical Physics* 120.3 (Sept. 2008), pp. 549–559. ISSN: 1347-4081. DOI: 10.1143/ptp.120.549. URL: http://dx.doi.org/10.1143/PTP.120.549.

[49] Max Tegmark. "Measuring Cosmological Parameters with Galaxy Surveys". In: *Physical Review Letters* 79.20 (Nov. 1997), pp. 3806–3809. ISSN: 1079-7114. DOI: 10.1103/physrevlett.79.3806. URL: http://dx.doi.org/10.1103/PhysRevLett.79.3806.

[50] Giuseppe Tormen. "Instabilità di Jeans: universi statici". In: *Dispense per il corso di Cosmologia Modulo A G.Tormen, Dipartimento di Astronomia, Università di Padova*.

[51] Jesus Torrado and Antony Lewis. "Cobaya: Code for Bayesian Analysis of hierarchical physical models". In: *arXiv e-prints*, arXiv:2005.05290 (May 2020), arXiv:2005.05290. arXiv: 2005.05290 [astro-ph.IM].

[52] Jesús Torrado and Antony Lewis. *Cobaya: Bayesian analysis in cosmology*. Oct. 2019. ascl: 1910.019.

[53] Christos G. Tsagas. "Cosmological Perturbations". In: *Lect.Notes Phys.592:223-261,2002* (2012).

[54] Luca Valenziano. *The Euclid Mission*.

[55] Velasquez-Toribio et al. *Observational constraints on the non-flat ΛCDM model and a null test using the transition redshift*. 2020. arXiv: 2001.04645 [astro-ph.CO].

[56] van de Weijgaert. *Chapter4: Linear Perturbation Theory*. 2009.

[57] Kazuhiro Yamamoto, Hiroaki Nishioka, and Yasushi Suto. "The Cosmological Light-Cone Effect on the Power Spectrum of Galaxies and Quasars in Wide-Field Redshift Surveys". In: *The Astrophysical Journal* 527.2 (Dec. 1999), pp. 488–497. ISSN: 1538-4357. DOI: 10.1086/308126. URL: http://dx.doi.org/10.1086/308126.

[58] Gong-Bo Zhao et al. "Dynamical dark energy in light of the latest observations". In: *Nature Astron.* 1.9 (2017), pp. 627–632. DOI: 10.1038/s41550-017-0216-z. arXiv: 1701.08165 [astro-ph.CO].

[59] P.A. Zyla et al. "Review of Particle Physics". In: *PTEP* 2020.8 (2020), p. 083C01. DOI: 10.1093/ptep/ptaa104.